



VNiVERSIDAD  
D SALAMANCA



# POLITECNICO DI TORINO

Master's Thesis in Mechanical Engineering

## Mechanical validation of the predict tensile behaviour of FDM made specimens

*Supervisors:*

*Prof. Chiandussi Giorgio*

*Ing. Tridello Andrea*

*Prof. Andres Sanz-Garcia*

*Candidate:*

*Cimino Maria Teresa*

*Ai miei genitori, Francesco e Norina,  
e a mia sorella Marta,  
io sono ciò che voi siete.*

# Contents

<b>Chapter 1: Introduction</b>	<b>7</b>
1.1. Additive Manufacturing	9
1.1.1. Fused Deposition Modeling	10
1.2. Objective of the project	12
1.3. Build parameters	13
1.4. State of art	16
1.5. Materials	18
1.5.1. Polylactic acid	18
1.5.2. Acrylonitrile Butadiene Styrene	19
1.5.3. Polycarbonate	20
<b>Chapter 2: Materials and Method</b>	<b>21</b>
2.1. Experimental data	21
2.1.1. Standard	22
2.1.2. Papers	23
2.2. Digimat software	27
2.3. Structural model	29
2.4. Material definition	32
2.5. Manufacturing data	35
2.6. Solutions settings	38
<b>Chapter 3: Results and discussion</b>	<b>40</b>
3.1. Curves Marc	40
3.2. Digimat model	42
3.2.1. Polylactic acid	43
3.2.2. Acrylonitrile Butadine Styrene	50
3.2.3. Polycarbonate	55

3.3. Experimental validation	59
<b>Chapter 4: Conclusions</b>	<b>66</b>
<b>Appendix</b>	<b>68</b>
<b>References</b>	<b>69</b>

## List of Figures

Figure 1. Fused deposition modelling process [5] .....	11
Figure 2. Build orientations [7] .....	14
Figure 3. Infill options, from the left: low, high and solid [9] .....	15
Figure 4. Build orientations and raster angles [11] .....	17
Figure 5. Specimen dimensions [16] .....	22
Figure 6. Engaguge Digitizer method [21] .....	24
Figure 7. Digimat main screen .....	28
Figure 8. Schematization of the model .....	29
Figure 9. Mesh realized in Marc .....	30
Figure 10. Boundary conditions: a) fixed displacement at the top surface b) Encastre at the bottom surface .....	31
Figure 11. Definition of a filament microstructure .....	33
Figure 12. Loading and printing directions .....	34
Figure 13. Idealized stress-strain response of a polymer under uniaxial tension in the x-direction .....	35
Figure 14. Input and output files of the mapping process .....	36
Figure 15. Association between STL and G-Code a) right superposition b) wrong superposition .....	37
Figure 16. The Digimat-RP ribbon .....	39
Figure 17. Stress-strain curves obtained using only Marc .....	41
Figure 18. Experimental VS Simulated stress-strain curves of Ferreira case study [20] .....	44
Figure 19. Experimental VS Simulated stress-strain curves of Chacon case study [7] .....	47
Figure 20. Experimental VS Simulated stress-strain curves of Rodriguez case study [19] .....	49
Figure 21. Experimental VS Simulated stress-strain curves of Riddick case study [11] .....	52
Figure 22. Experimental VS Simulated stress-strain curves of Cantrell case study [17] .....	54
Figure 23. Experimental VS Simulated stress-strain curves of Domingo case study [15] .....	56
Figure 24. Experimental VS Simulated stress-strain curves of Salazar case study [14] .....	58

Figure 25. Specimens anchored to the platform: a) horizontal specimens b) vertical specimens top view c) vertical specimens 3D view .....	60
Figure 26. ElectroForce 3500 series Universal testing machine .....	61
Figure 27. PLA test specimens tested .....	61
Figure 28. a) Fracture surface b) infill option .....	62
Figure 29. Simulated VS Experimental curves of horizontal samples tested in laboratory.....	63
Figure 30. Defects of vertical printed component: on the top, different in the filament deposition; on the bottom, contour problems .....	64
Figure 31. Different infill: a) printed specimen b) from Cura software.....	64
Figure 32. Experimental curve of vertical sample tested in laboratory .....	65
Figure 33. Effect of the residual stresses.....	68

## List of Tables

Table 1. Papers selected for this investigation.....	24
Table 2. Mesh convergence .....	31
Table 3. Materials properties.....	41
Table 4. Ferreira et al.'s build parameters [20] .....	43
Table 5. Chacon et al.'s build parameters [7].....	46
Table 6. Rodriguez et al.'s build parameters [19].....	49
Table 7. Riddick et al.'s build parameters [11] .....	51
Table 8. Cantrell et al.'s build parameters [17] .....	54
Table 9. Domingo et al.'s build parameters [15].....	55
Table 10. Salazar et al.'s build parameters [14].....	57
Table 11. Printing parameters of the laboratory test [19].....	60

## Abstract

In recent years, the field of additive manufacturing has evolved rapidly in terms of objects complexity, materials, manufacturing times, components already assembled, etc. The objective of the project is to work on the characterization of components manufactured by fused deposition modeling (FDM) showing properties that can be influenced by several parameters. Herein, the most important ones are studied by using simulations that combine MSC and DIGIMAT software following two different approaches: macro-scale and material's mesostructure-based analysis. The main components of this work will be the finite element method (FEM) as a useful tool for the validation, and the stress-strain values from the experimental data found in the literature or gathered from laboratory tests. The final goal is to predict the mechanical response of the 3D printed components and relate their mechanical properties with the build parameters.

# Chapter 1: Introduction

The aim of this work is to study the tensile properties of FDM made test specimen considering the main build parameters. The first chapter is dedicated to a detail description of the considered additive manufacturing process and a review of the state of art. The most significant printing parameters have been identified. Among these, the ones that are considered more relevant are the following: build orientation, layer thickness, raster angle, infill density. Previous works highlight the influence of these parameters on mechanical properties by experimental tests in order to characterize the mechanical performance of samples manufactured by FDM. In the case of this study, only tensile behaviour is going to be investigated. The main goal is to predict the response of 3D printed components without testing them. This objective has been achieved through coupled analysis between DIGIMAT and a structural FEA solver that in this study, is Marc Mentat.

DIGIMAT is a software which enables to bridge the gap between the processing simulation and the finite element solver. Shortly, DIGIMAT permits multi-scale material's approaches in an integrative, accurate and efficient way. In addition, the structure modeling is also enabled by considering the process-induced material microstructure in the FEA of the final part structure [1]. Consequently, the starting point of the process is the use of structural models

obtained in Marc, which is going to be integrated with the material definition and further simulation.

Regarding the material definition, with the latest DIGIMAT versions it is possible to study the effect of the printing pattern and porosity on materials behaviour by defining the filament microstructure. Other aspect to consider in the simulation of FDM is the manufacturing data namely the toolpath information which can be exported from a slicing software. The necessary files are the STL and the G-Code files. Once manufacturing data has been defined, a mapping step is required. At the end of the definition component workflow, it is possible to launch the coupled analysis with the FEA solver and open the result files in Marc. To validate the stress-strain curves, values from literature and laboratory tests will be used.

## 1.1. Additive Manufacturing

Additive manufacturing is the process of building three dimensional (3D) parts by adding layers of material [2]. In the scope of new production technologies, it certainly has a significant importance thanks to the innovative way of manufacturing. This technique enables the fabrication, in few hours and without the use of expensive equipment, of components with a complex geometry. In contrast to the conventional technologies, which work by material subtraction from the raw, additive manufacturing is based on the material deposition layer by layer. It has initially been developed for prototypes production and for this reason it is also known as Rapid Prototyping. Recently, the application of additive manufacturing has increased exponentially and nowadays it's widespread the production of definitive pieces. This rapid development is due to the advantages that can be achieved by additive manufacturing such as reduced part counts, freedom during the design stage and components lightening. Other important aspects are the absence of tooling and the product lifecycle: reduced cost and time to market. Applications are present in many fields, for example medical and dental applications are very common thanks to the possibility of customization; as well aerospace sector

where the use of lightweight components allows the reduction of the costs and pollutant wastes.

There are many AM technologies that can be grouped into seven categories based on processes that are defined in ASTM F2792 [3]: vat photopolymerization, material jetting, binder jetting, power bed fusion, material extrusion, directed energy deposition, and sheet lamination.

Each process is different from the others because of its specific technological features but there are some shared principles. First, the printable model can be created with a computer aided design (CAD) program and saved with stereolithography file format (STL). Before printing a 3D model from an STL file, this must be examined for errors like holes, self-intersections and faces normal. At this point, there is the orientation in the machine, the supports creation and the 'slicing' software transforms the model into a series of thin layers. Once this has been completed, the component is ready to be 3D printed. The materials used for additive manufacturing are very diverse, including polymers, metals, composites and ceramics and the feedstock can be different based on the process used. The choice of the process and the material depends on final properties desired for the component to be printed.

### 1.1.1. Fused Deposition Modeling

One of the most common additive manufacturing techniques is Fused Deposition Modeling (FDM) that belongs at ‘Material extrusion’ type and it was patented by the founder of Stratasys over 20 years ago. As shown in Fig. 1, the FDM uses a heating chamber to liquefy polymer that is fed into the system as a filament. The filament is pushed into the chamber by a tractor wheel arrangement and it is this pushing that generates the extrusion pressure [4].

The molten material is extruded by a nozzle which can be moved across the XY plane. Once a layer is completed, the platform is lowered in the Z direction in order to build the object layer by layer.

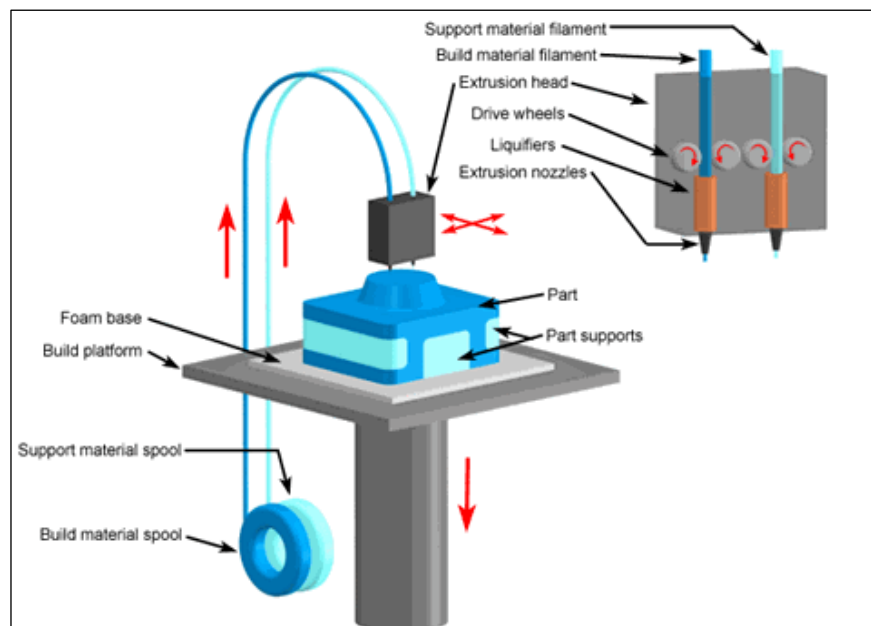


Figure 1. Fused deposition modelling process [5]

The most common materials used for FDM are the thermoplastic polymers that becomes mouldable at high temperature and solidifies upon cooling.

In case of objects with cavities or protruding parts, support structures may be generated. A different nozzle is used for these parts which can be made by another material.

There are two types of support material available, soluble and breakaway. The type of support material used is dependent on the model material being printed. While several model materials require break away supports, most materials use the soluble support or can use both. The soluble support material can either be removed by hand or dissolved in a bath of sodium hydroxide [6].

The FDM process is cheaper than the other additive manufacturing processes and there aren't installation constrains since the feedstock does not present criticalities as the powders and resin.

## **1.2. Objective of the project**

The aim of this work is to characterize components manufactured by FDM and to predict the mechanical response of these components as a function of the aforementioned build parameters. Despite the use of additive manufacturing is in continuous expansion, the uncertainty on the mechanical

properties of printed parts hinders its full development. Another drawback is related to its higher manufacturing costs than the traditional manufacturing techniques. For this reason, it is very important to know how the individual parameters affect the 3D printed component to optimize their processing and their structure. Two different approaches are going to be used: the macro-scale and the material's meso structure analysis.

The finite element method (FEM) will be used for the validation and for the experimental data, values of stress-strain from literature will be used. The work will be done using both simulations software: Marc and Digimat. The first one provides nonlinear finite element analysis to simulate the product behaviour. Digimat is a multi-scale material modelling technology. It should be pointed out that in this script only the influence of parameters on tensile strength will be considered though it also can be observed variations on compressive strength, flexural strength and impact behaviour.

## 1.3. Build parameters

Parameters that affects the properties of the 3D printed components are related to the process of Fused Deposition Modelling, also known as Fused Filament Fabrication. The most important parameters are the following:

- Build orientation: all commercial 3D printers have a chamber with specific dimensions that can be assimilated to a parallelepiped. There

are three possible directions along which a specimen can grow up on the platform. In this work they will be named as follows: Horizontal (or Flat) and On-edge, where the fused filament deposition is positioned in the same direction as the pull direction and Upright (or Vertical) in which layers were deposited perpendicular to the pull direction [7]. Fig. 2 shows an example.

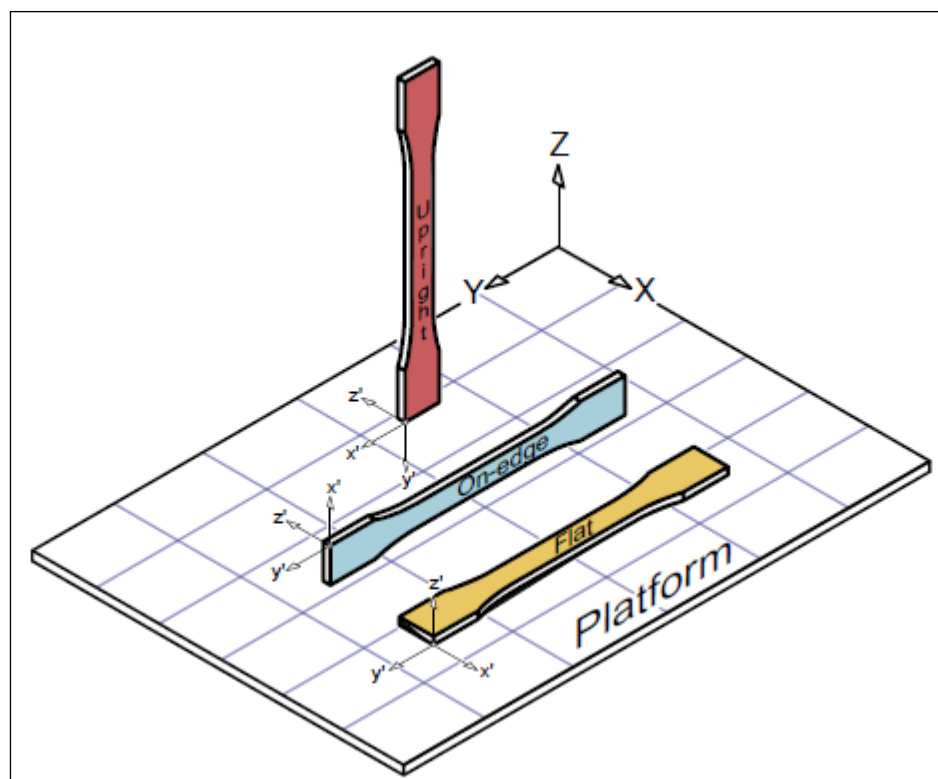


Figure 2. Build orientations [7]

Regarding the print orientation, in the present work, the samples are all aligned with the Y-axis;

- Raster angle: inclination of the filament respect to a reference direction that usually is the load direction;

- Layer thickness: thickness of any single layer that depends on that of the deposited bead. Large values of layer thickness reduce the production time and consequently manufacturing costs but increase the shrinkage and the residual stresses.;
- Air gap: distance between two adjacent deposited filaments of the same layer. The default value is usually zero, meaning that the beads touch each other. A possible alternative is a positive gap, meaning that a gap is present between adjacent rasters, or a negative gap, implying that the bead tracks are overlapped [8]. This parameter can be evaluated by percentages or by infill options like: low, high and solid (Fig. 3).



*Figure 3. Infill options, from the left: low, high and solid [9]*

There are other aspects that can influence the properties, i.e. number of contours, feed rate but in this work only those listed above are going to be analysed.

## 1.4. State of art

As shown in the paragraph 1.3., there are a lot of parameters that are influential. Mechanical properties of a piece produced by FDM are generally lower than the original material or that the same piece produced by injection moulding. In fact, AM technology can generate parts with porosity, anisotropic properties and residual stresses. Several authors studied the influence of these parameters on the mechanical properties and a general response is that the highest resistance occurs when the filament deposition has the same direction as that of traction. Ahn et al. [11] show the influence of raster orientation and air gap of flat specimens tested under axial load. Maximum strength is obtained when the beads are deposited parallel to the load direction while the value is minimum when filaments are perpendicular to the applied force. The authors also discovered how bead width hasn't a great effect. Other parameter investigated was the air gap that can influence strength and production time. Specimens with high porosity are faster to produce than solid specimens but have low strength.

Chacòn et al. [7] define the effects of build direction and layer thickness on tensile strength. They define two main failure modes: inter-layer failure and trans-layer failure. In the first case, layer or fibre-to-fibre adhesion significantly affected tensile strength while in trans-layer failure fibre breakage was observed. Upright samples exhibited inter-layer failure with

lower strength and stiffness performance. On the other hand, on-edge and flat samples showed trans-layer failure with the highest mechanical properties. In addition, the results have highlighted brittle fracture behaviour for the upright orientation and ductile fracture behaviour for the on-edge and flat orientations. Regarding layer thickness, this parameter has a different effect as a function of the build direction. In upright samples, tensile strength increases as layer thickness increases. In cases of flat and on-edge samples the strength increases for a medium value of layer thickness but then decreases as the thickness increases. Moreover, a parametric analysis of the process parameters is performed.

Another parameter that should be investigated is the raster angle, Riddick et al. [11] investigate a range of specimens at different build direction and raster orientation:  $\pm 45^\circ$ ,  $0^\circ$ ,  $0/90^\circ$ , and  $90^\circ$  as shown in Fig. 4.

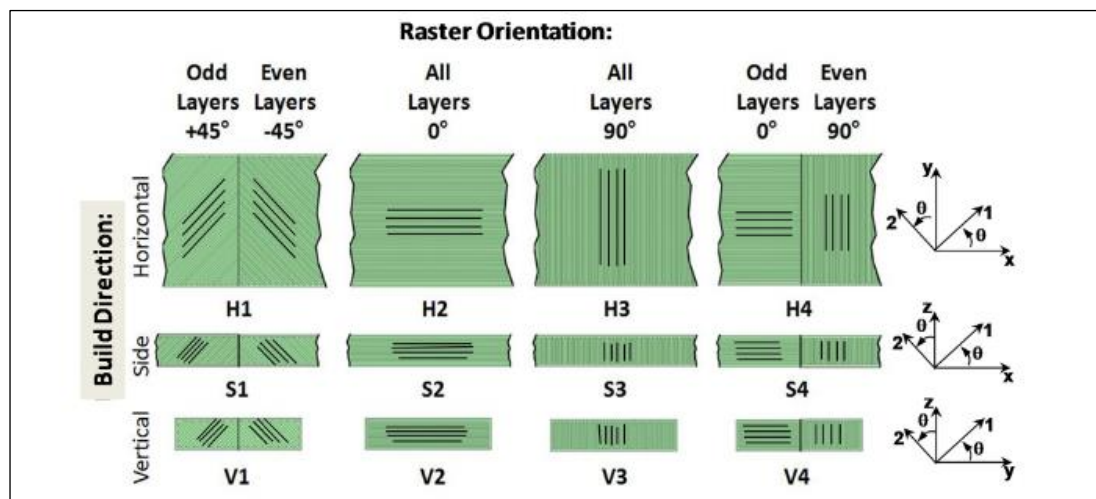


Figure 4. Build orientations and raster angles [11]

They discovered that  $\pm 45^\circ$  horizontal specimen was characterized by evident softening due to the shear response, resulting in the greatest elongation-at-break value of all the specimens tested. Furthermore, fractographic analysis carried out during their work show that the side build specimens make better use of the geometry of the raster to fill the voids between rows.

Ravindrababu et al [10] consider the influence of build and print orientations. They noticed that build orientation has a larger impact than print orientation on the elastic deformation of an FDM printed part.

## 1.5. Materials

Thermoplastic polymers are the most common materials printing via FDM. These materials are plastic polymers that are flexible and resistant to room temperature, but they soften at high temperature. In general, the polymer is in the form of a filament fabricated from virgin resins. Polymers that can be used are various i.e. polylactic acid (PLA), acrylonitrile butadiene styrene (ABS), polycarbonate (PC), PEEK, Ultem, PETG.

For this work, only the first three materials are going to be studied because they are the most used for experiments and consequently those for which there are more curves stress-strain.

### **1.5.1. Polylactic acid**

Polylactic acid (PLA) is a biodegradable and bioactive thermoplastic which allows to have zero disposal costs. PLA is derived from renewable resources, such as corn starch, sugar cane, tapioca roots or even potato starch. During the melting phase PLA doesn't emit vapour or fumes and it is water-soluble. This material is used for biomedical purposes and in food packaging, bags, disposable tableware, upholstery, disposable garments, hygiene products: therefore, it is considered as safe. PLA is tough, but a little brittle, once it has cooled down. Its temperature threshold is lower than the one of ABS, as PLA is normally extruded around 160°C-220°C. The tensile strength is larger than ABS, but it has a lower ductility.

### **1.5.2. Acrylonitrile butadiene styrene**

Acrylonitrile butadiene styrene (ABS) is a very common material used to produce FDM parts. It is a thermoplastic material characterized by different weights of the three main monomers and by changing the percentage of these, it's possible to customize it. This material is very strong and durable, flexible and quite resistant to heat. ABS is used in a very large variety of applications in the industry nowadays. Examples are pipes, automotive components, electronic assemblies, protective headgear, protective carrying cases and toys.

The ABS-M30 produced by Stratasys is up to 25 to 70 percent stronger than other ABS-based products. Layer bonding is significantly stronger than that of standard ABS, for a more durable part. This results in more realistic functional tests and higher quality parts for end use [13].

### **1.5.3. Polycarbonate**

Polycarbonate (PC) is a more recent material characterized by a high impact resistance and low shrinkage. It is easily worked, moulded, and thermoformed. PC is suitable for printing components having a complex geometry because it doesn't drool. Unlike most thermoplastics, PC has very high elongations at break and for this reason it can be processed and formed at room temperature. It provides reasonable mechanical properties and heat resistance. It is widely used in automotive, aerospace and medical applications [14].

## Chapter 2: Materials and Method

Chapter 2 is dedicated to a detail explanation of the steps followed for the method and material definitions. First, the most interesting papers for this type of work have been selected and all the data of the curves collected. Thereafter, each step of the proposed model has been showed so that it is repeatable and clear.

### 2.1. Experimental data

Stress-strain curves analysed are obtained by literature. Scientific digital database provides many papers for this type of work in which specimens, with different parameters and printed by FDM, were tested. These papers have been selected according to the standard used for the experiments. ASTM standard was preferred instead of ISO because it is the standard used by the manufacturer of the specimen material and for most of the authors studying the mechanical behaviour of AM parts, too [15]. For this reason, it has been decided to use only papers that follow ASTM D638 in order to facilitate the comparison of the results obtained with the certainty that everything was done following this standard.

### 2.1.1. Standard

ASTM D638 is the standard test method for tensile properties of plastics that covers the determination of the tensile properties of unreinforced and reinforced plastics in the form of standard dumbbell-shaped test specimens when tested under defined conditions of pre-treatment, temperature, humidity, and testing machine speed [16]. The standard explains the procedure and the apparatus to use. The test specimen shall conform to the dimensions shown in Fig. 5.

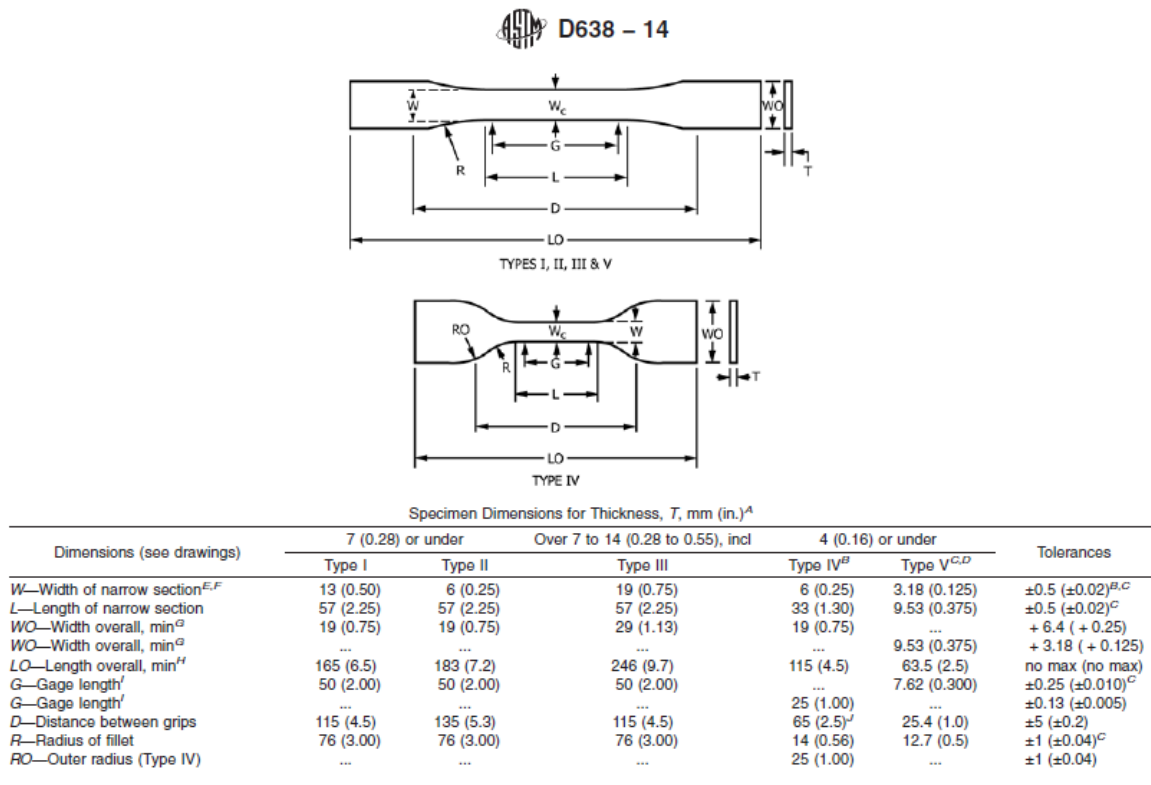


Figure 5. Specimen dimensions [16]

In general, if the shape of the material falls into the sheet stock category and meets a minimum thickness requirement, then Type I specimens are recommended for most materials. Type II through Type V specimens are generally only used when there is insufficient material of the required thickness or shape to make Type I specimens [6]. Papers that have been found during the investigation use Type I as reported in the Table 1.

### 2.1.2. Papers

In research, only papers written in English were chosen and the following keywords have been used: (“FDM” or “Fused Deposition Modeling”) and (“parameters”) and (“tensile test” or “mechanical behaviour”). The most recent papers have been selected. They have been reported in Table 1.

	<i>Material, Specimen Type</i>	<i>Variable parameters</i>
<i>Riddick, 2016 [11]</i>	ABS, Type I	Build direction, raster angle
<i>Cantrell, 2017 [17]</i>	ABS, Type I	Build direction
<i>Samykano, 2019 [18]</i>	ABS, Type I	Layer thickness, raster angle, air gap
<i>Croccolo, 2013 [8]</i>	ABS, Type I	Build direction
<i>Rodriguez, 2018 [19]</i>	ABS and PLA, Type I	Build direction, layer thickness, air gap
<i>Ferreira, 2017 [20]</i>	PLA, Type I	Raster angle
<i>Chacon, 2017 [7]</i>	PLA, Type I	Build direction, layer thickness

<i>Salarz-Martin, 2018 [14]</i>	PC, Type I	Air gap
<i>Domingo, 2015 [15]</i>	PC, Type I	Build direction

Table 1. Papers selected for this investigation

All these papers report stress-strain curves obtained by tensile test on specimens on which the parameters changed. First of all, the graphs in the papers have been transformed into image files (.PNG) and subsequently converted by Engauge Digitizer. This tool accepts image files containing graphs and recovers the data points from those graphs by placing points along axes and curves [21]. Data can be transferred to other software, in this case Excel tabs have been created using copy and paste. Fig. 6 shows the logic procedure.



Figure 6. Engauge Digitizer method [21]

After editing all the curves, three different ‘.csv’ files for each paper have been created: the first one is the ‘metadata.csv’ where are reported all the papers, the second one is the ‘Author’s name\_m.csv’ contain the metadata describing the parameters changed during the experiment (raster angle, air gap etc.) and the last one is the ‘Author’s name\_d.csv’ storing the data obtained by Engauge

Digitizer. The first is unique while the other two are different for each paper. These files are going to be recall by a Python script which can be used to work with JSON data. The latter is a lightweight data-interchange format that in this case has been used to store the data. The name derived from JavaScript Object Notation and it has had a wide spread because it is easy for humans to read and write. Below is reported the Python script.

```
import csv
import json
import pandas as pd

# Main inputs to be filled
# Function to read experiments and data and particular metadata from them

def reading_values(dictionary, file_name):
    data = pd.read_csv('C:\\Users\\Maria Teresa\\Desktop\\python\\data\\' + file_name + '_d.csv',
delimitter=',')
    meta = open('C:\\Users\\Maria Teresa\\Desktop\\python\\data\\' + file_name + '_m.csv', 'r')
    reader = csv.reader(meta)
    header = next(reader)

    # print(header)

    output = {}
    i = 0
    for row in reader:
        output = {
            '@id': row[0],
            'build_orientation': row[1],
            'print_orientation': row[2],
            'layer_thickness': row[3],
            'density_infill': row[4],
            'raster_angle': row[5],
            'young_modulus': row[6],
            'values': []
        }

    # list_experiments = int(output['number_experiments'])
    #for experiment in range(list_experiments):

    e = data.iloc[:, 0 + i * 2]
    s = data.iloc[:, 1 + i * 2]
    output['values'] ={'e': pd.Series.tolist(e), 's': pd.Series.tolist(s)}
    i = i + 1
    dictionary[file_name]['experiments'].append(output)
    return dictionary
```

*# Function to read the general metadata from one paper.*

```
def reading_metadata(filename):
f = open('C:\\Users\\Maria Teresa\\Desktop\\python\\data\\' + filename + '.csv', 'r')
reader = csv.reader(f)
header = next(reader)
print(header)
output = {}
for row in reader:
output[row[0]] = {
    '@uid': row[1],
    'paper': row[2],
    'test_machine_kN': row[3],
    'test_velocity_mm_min': row[4],
    'type_printer': row[5],
    'type_ASTM': row[6],
    'material': row[7],
    'provider_material': row[8],
    'add_info': row[9],
    'link': row[10],
    'doi': row[11],
    'experiments': []
}
return output
```

*# Main part of the script*

```
metadata_name = 'metadata'
```

*# Name of the whole and large data*

*# To read the metadata of one .csv with the following structure:*

*# @uid,authors,material,test\_machine,type\_printer,type\_specimen,provider\_material,add\_info,link,doi*

```
meta = reading_metadata(metadata_name)
```

```
with open('C:\\Users\\Maria Teresa\\Desktop\\python\\output\\' + metadata_name + '.json', 'w') as
file:
```

```
    json.dump(meta, file)
```

*# To read both the experimental data and the particular metadata from two different .csv.*

*# The structure of the metadata (\_m.csv) is as follows:*

*# @id,build\_orientation,layer\_thickness,density,raster\_angle,print\_speed,strain\_rate,young\_modulus*

*# The structure of the data (\_d.csv) is as follows:*

*# e.g. e\_1;s\_1;e\_2;s\_2;e\_3;s\_3*

```
file_name = 'Cantrell_1' # Name of the particular paper that you want to process
```

```
with open('C:\\Users\\Maria Teresa\\Desktop\\python\\output\\' + metadata_name + '.json', 'r') as
file:
```

```
    dictionary = json.load(file)
```

```
    meta_with_data = reading_values(dictionary, file_name)
```

```
with open('C:\\Users\\Maria Teresa\\Desktop\\python\\output\\' + metadata_name +
'_with_experiments.json', 'w') as file:
```

```
    json.dump(meta_with_data, file)
```

## 2.2. Digimat software

The goal of this project, as anticipated before, is to use Digimat to predict mechanical behaviour of component printed by FDM. More than just software, Digimat allows users do both micro- and macro-scale analyses of composites and homogeneous material, predicting their behaviour in an intuitive way. The objective of Digimat is also to close the gap between manufacturing process and structural analysis through coupled analysis with structural FEA process.

The latest versions offer a holistic simulation platform for additive manufacturing that delivers a unique combination of material engineering, process simulation, and structural analysis solutions [22]. This represents a great potential since there is still much to know about behaviour of components produced by this process.

The multi-scale software modeling platform is shown in Fig. 7. It can be seen that there are two different interfaces for the users [23]:

- 1) Tools: set of software focused on material engineering (Digimat-MF and Digimat-FE) and structural engineering (Digimat-MX, Digimat-MAP and Digimat-CAE); these products focusing on expert usage;
- 2) Solutions: using the technology present in Digimat Tools this methodology simplifies the sequence of tasks with the help of intuitive

and user-friendly interfaces (Digimat-RP, Digimat-HC, Digimat-VA and Digimat-AM).

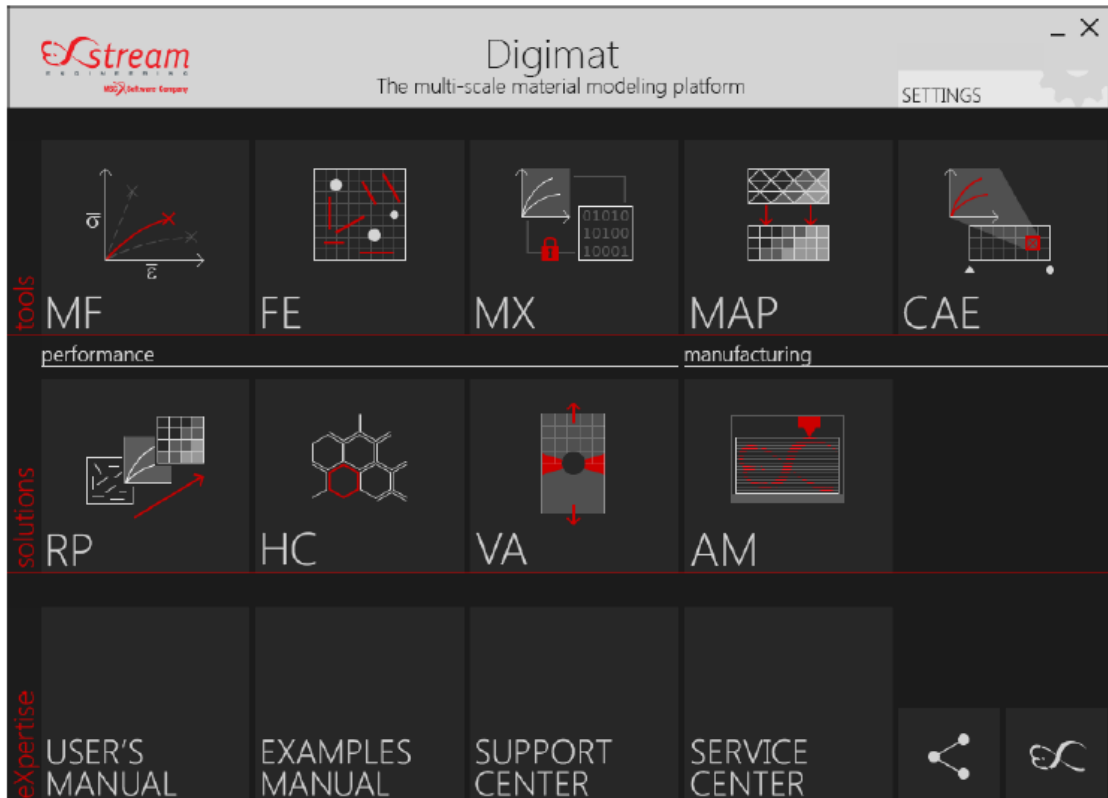


Figure 7. Digimat main screen

Obviously, not all the tools are going to be used but the path followed in Fig. 8 is the one that best simulates the model and optimizes results. In the paragraphs below all of these aspects will be investigated in detail.

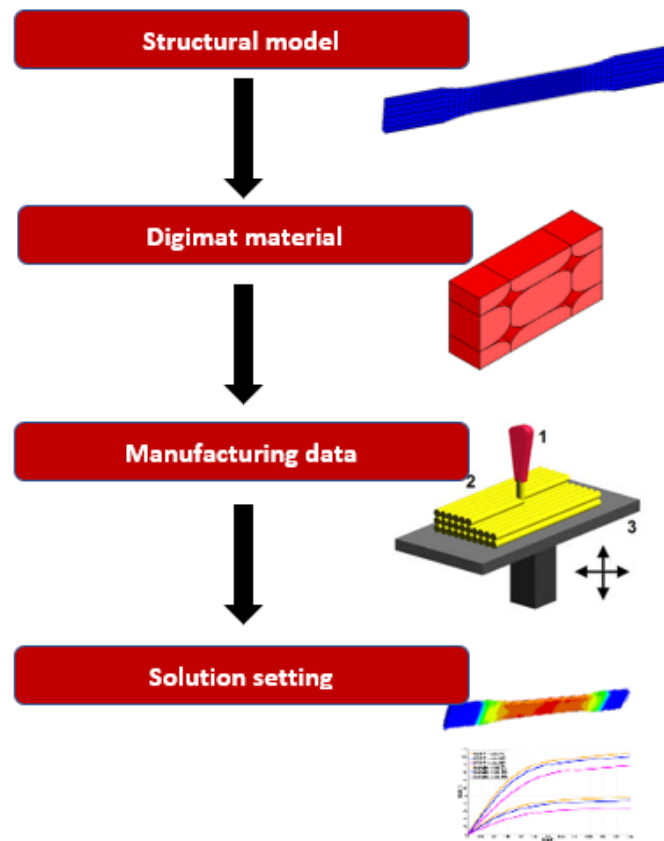
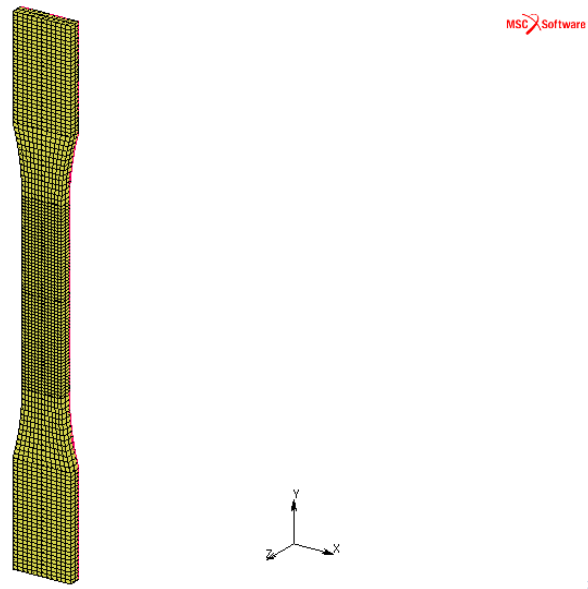


Figure 8. Schematization of the model

## 2.3. Structural model

Digmat allows coupled multi-scale analysis of several FEA solvers such as: Abaqus, Ansys, Marc, Nastran etc. In this work, Marc Mentat 2018 has been used because it integrates better with Digmat being of the same manufacture. So, for the moment it is the one that provides the best results.

First of all, the geometry of the specimen has been defined by following the ASTM Standard Type I and the mesh has been created as it is possible to see in Fig. 9.



*Figure 9. Mesh realized in Marc*

The material assigned to the specimen is an elastoplastic material. The Young's modulus, the Poisson's ratio and the Yield stress have been assigned. The materials studied, as anticipated in the Section 1.5 are three and for each, different parameters were introduced.

The aim of this structural model is to simulate a tensile test and obtain the mechanical characterization of the specimens. For this reason, the boundary conditions have been defined as follows:

- Encastré at the bottom surface;

- Fixed displacement at the top surface.

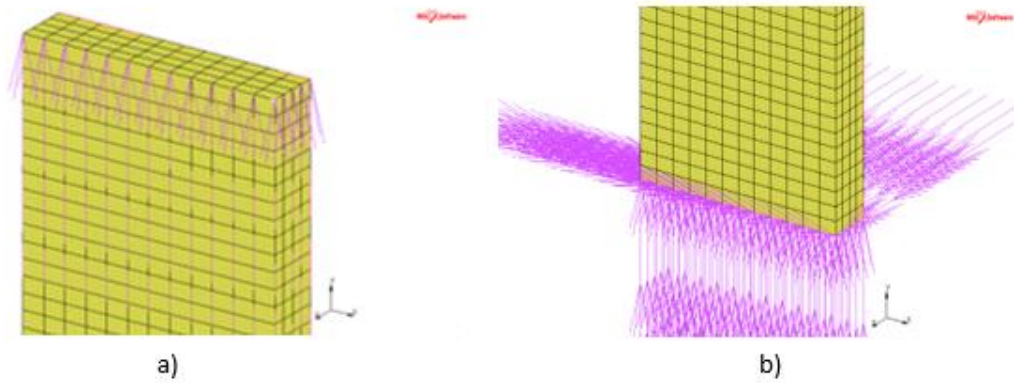


Figure 10. Boundary conditions: a) fixed displacement at the top surface b) Encastre at the bottom surface

Once all input parameters are defined, jobs can be launched, and finally the results will be analysed. One of the most important issues in Finite Element Analysis is the mesh convergence in order to ensure that the results are not affected by changing the size of the mesh. Hence, the initial mesh has been subdivided many times and it has been studied the relative standard deviation of the equivalent Von Mises stress in a central point of the geometry. In Table 2, these values have been reported and as it can be seen, the converge is achieved with the smaller mesh and the computational time is reduced.

	<i>Number of nodes</i>	<i>Equivalent Von Mises stress at the centre node [MPa]</i>	<i>Relative standard deviation [%]</i>
<i>Mesh 1</i>	5655	80.41	-
<i>Mesh 2</i>	52311	80.21	0.25
<i>Mesh 3</i>	425559	80.16	0.31

Table 2. Mesh convergence

The structural model definition has two purposes, the first one is to know the mechanical behaviour of a solid specimen not affected by FDM parameters and, the second one is having the '\*.dat' files that are the input for Digimat analysis.

## 2.4. Material definition

The second step is the material definition. In Digimat there are three different tools which support AM material needs:

- Digimat-MF, this tool enables the prediction of the constitutive behaviour of heterogeneous and/or anisotropic materials by using a Mean-Field homogenization method;
- Digimat-FE, to perform FEM of realistic Representative Volume Elements (REV);
- Digimat-MX, that is a Material eXchange platform to reverse engineering, store and exchange material models between suppliers and users [1].

In the case of this investigation, Digimat-MF is going to be adopted. The main advantages over Digimat-FE are the ease of use, the speed (low CPU time), and reduced memory usage even if is more approximate [1]. Nevertheless, the material studied is homogeneous and with low complexity level to be examined in detail. For this reason, the calculation speed was privileged.

The material studied is homogeneous but the inter-bead porosity (typical of additive manufacturing) could generate anisotropy in the material response. Digimat-MF allows to define a Lattice microstructure that is a user-defined definition of the cross-section of unreinforced filament. This microstructure can be characterized through the definition of: ratio between extrusion width and layer height, relative bonded width and relative bonded height. Once these values are set, the porosity is automatically computed, and a 3D visualization becomes available as shown in Fig. 11.

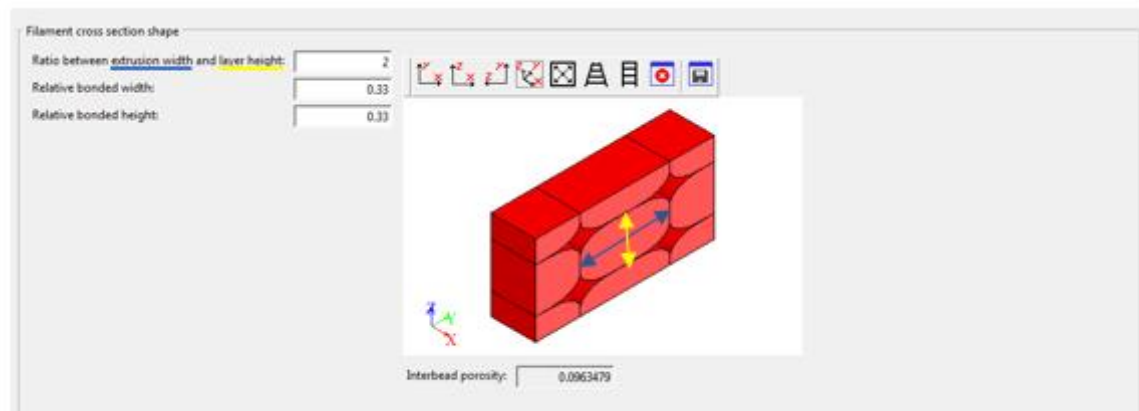


Figure 11. Definition of a filament microstructure

Other important aspects in the material definition (Fig. 12) are the printing and the loading (in this case, mechanical) directions since the results are affected from these values.

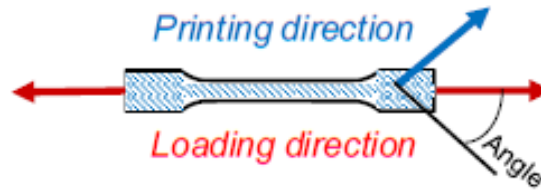


Figure 12. Loading and printing directions

For each case study, the material constants (i.e. Young's modulus, Poisson's ratio, yield stress etc.) have been changed to be consistent as far as possible with the different papers. The material is always elastoplastic, and the model used is the J2-plasticity that is based on the von Mises equivalent stress  $\sigma_{eq}$ .

$$\sigma_{eq} = \sqrt{J_2(\sigma)} \quad \text{Equation 1}$$

where:

$$J_2 = \frac{1}{2} [(\sigma_{11} - \sigma_{22})^2 + (\sigma_{22} - \sigma_{33})^2 + (\sigma_{33} - \sigma_{11})^2] + 3[\sigma_{12}^2 + \sigma_{23}^2 + \sigma_{13}^2]$$

Equation 2

As shown in Fig. 13, the response of this model is linear elastic as much as the equivalent stress is less than the initial stress yield. When this inequality is no longer respected, plastic deformation appears.

The total strain observed by the material is assumed to be the sum of the plastic strain and the elastic strain.

$$\varepsilon = \varepsilon^e + \varepsilon^p \quad \text{Equation 3}$$

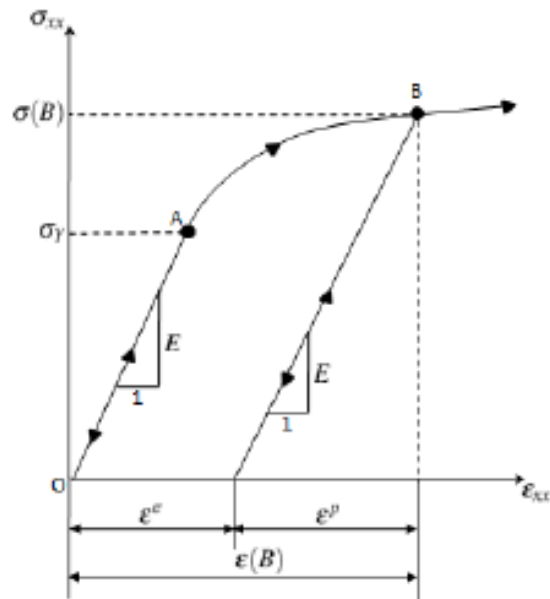


Figure 13. Idealized stress-strain response of a polymer under uniaxial tension in the x-direction

Once the job has been launched, results are available and, the file \*.daf generated in Digimat-MF is the one that will be used in the Digimat-RP for the material definition of the component realized in Marc Mentat.

## 2.5. Manufacturing data

Components produced by FDM are affected by printing parameters, therefore the structural model should be customized to the latter ones. This process consists in a mapping solution to transfer data between dissimilar meshes. In the case of this investigation, the objective is to map the toolpath, that is the path followed by the printer head, to the structural FEA mesh. In Digimat, it is possible to use Digimat-Map that is the 3D mapping tool (that uses Digimat-

CAE as interface) or directly Digimat-RP. In both cases, to start the mapping process, it is mandatory to have ready the following:

- A donor mesh, that is the geometry (\*.stl file) to which the toolpath (\*.gcode) is associated;
- A receiving mesh (\*.dat), that is the structural mesh of which has been widely discussed in Paragraph 2.3.

This process is outlined in Fig. 14.

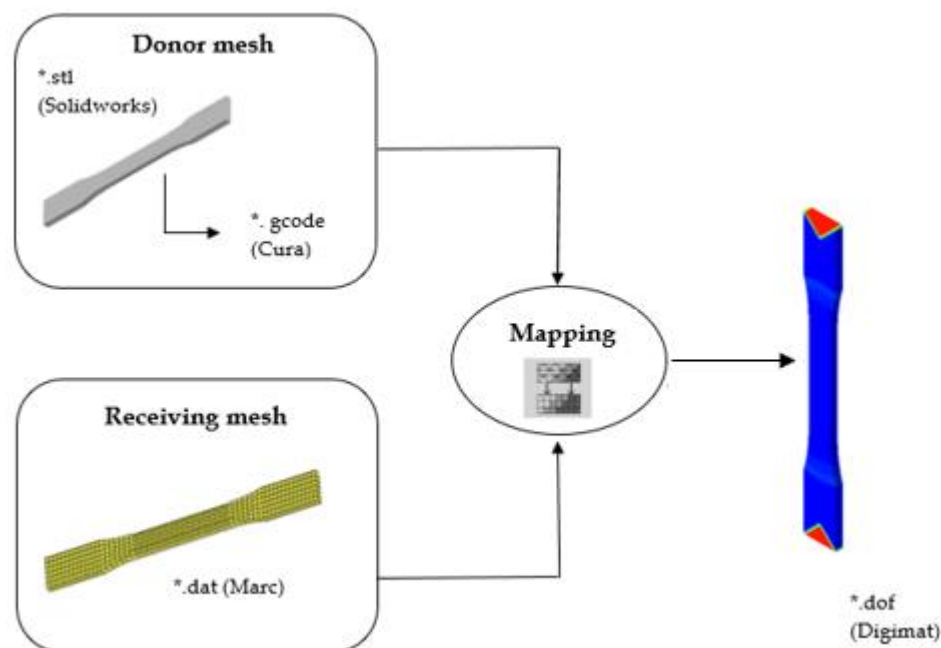


Figure 14. Input and output files of the mapping process

The STL has been generated on SolidWorks following Type I specimen dimensions, while the Cura software was used to assign printing properties (i.e. infill density, raster angle, layer thickness, speed rate etc.) and export the gcode files. It is important to specify that if a building directions study is required, it is

not enough to rotate the STL on Cura, but it is mandatory to draw the piece already in the right direction. In Fig. 15 this type of problem is highlighted. In grey it is possible to see the STL, while the red lines represent the toolpath. If these two do not match, the solution is not acceptable since there are not differences between the three different orientations.

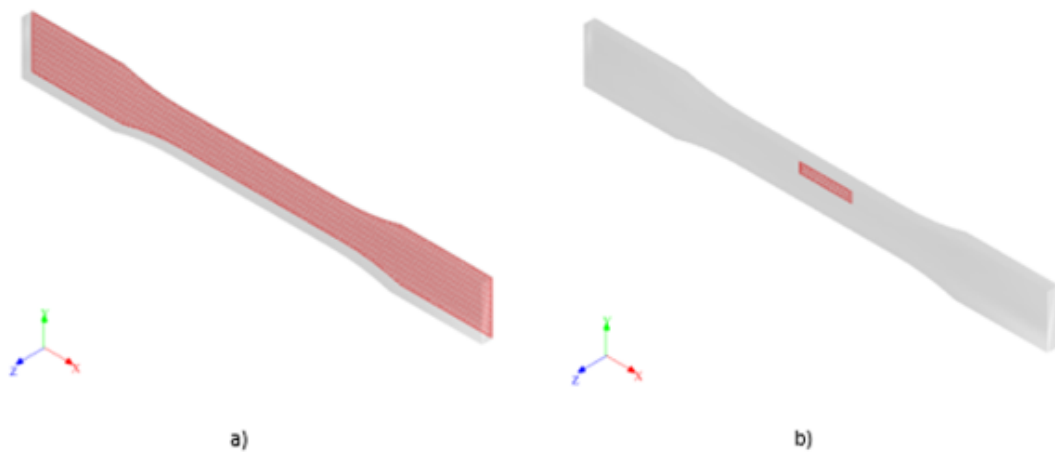


Figure 15. Association between STL and G-Code a) right superposition b) wrong superposition

All the transformations are performed on the donor mesh because the receiving one cannot be modified due to the boundary conditions definition and some other input of the structural FEA. The path followed can be summarized as follows: the toolpath is discretized in many points, and each point is assigned as information the orientation of the toolpath at that location. Each receiver element is then assigned a local orientation tensor corresponding to the set of orientations of the discretization points located inside that element. Elements containing no discretization point are assigned an averaged orientation tensor depending on

the orientation tensors of the neighbouring elements. Elements containing no discretization point that are completely disconnected from the elements intersecting the toolpath are not assigned any orientation data [1].

One news of the latest Digimat versions is that there is Digimat-AM software that simulates the printing process and predicts the warpage, residual stresses, temperature history and microstructures change in a printed part. In this work could be interesting to study the effect of the residual stresses after the printing process. This can be done mapping not only the toolpath but also these residual stresses to the structural model (see Appendix).

## 2.6. Solutions settings

Once all the input files have been generated, by using Digimat-RP it is possible to bridge the gap between simulations and predictions carried out on the structural side. In fact, through this integrated workflow environment, results files are generated, and they can be opened using Marc later. Another pipeline is to use Digimat-CAE that is the main tool for building coupled multi-scale analyses. In this case, the coupled Digimat-CAE/Marc analyses can only be executed on Windows platforms using commands in the command prompt. Furthermore, the structural input deck needs to be modified manually. In this project, Digimat-RP has been chosen to perform all the simulations.

The workflow navigation contains tabs related to the four steps which have been described until now, as shown in Fig. 16.



*Figure 16. The Digimat-RP ribbon*

Hence, the path to follow is intuitive and straightforward and it allows to easily customize the structural model. The first required file is the structural model to which the Digimat Material and the Manufacturing data will be added.

## Chapter 3: Results and discussion

This chapter is devoted to the description of the results obtained from the simulations and their comparison with the experimental ones. In addition, a laboratory test was conducted to make a significative comparison between numerical and experimental approaches.

### 3.1. Curves Marc

The first results are related to the solid specimen (as if they were made by injection moulding) obtained using only Marc. To determinate the stress-strain curves, the reaction force  $F$  at the bottom was calculated and then divided by the cross-sectional area  $A$  of the dog bone specimen, to calculate the stress  $\sigma$ .

$$\sigma = \frac{F}{A} \quad \text{Equation 4}$$

Regarding the strain, according to the ASTM standard [16], the displacement  $\Delta L$  was determined between two designated points within the gauge length of the test specimen. The strain  $\varepsilon$  (Eq. 5) is evaluated dividing this value for the initial length  $L$  that in Type I specimen is 50 mm:

$$\varepsilon = \frac{\Delta L}{L} \quad \text{Equation 5}$$

Table 3 shows the main parameters of the materials.

<i>Material</i>	<i>Young's modulus, MPa</i>	<i>Poisson's ratio</i>	<i>Yield stress, MPa</i>	<i>Elongation at break, %</i>
PLA [24]	3430	0.36	66.15	7
ABS-M30 [8]	2400	0.35	33	4
PC [25]	2390	0.32	62.7	83

Table 3. Materials properties

In Fig. 17, data obtained from finite elements analysis are plotted on a stress-strain graph to evaluate the differences from the behaviour of FDM specimens.

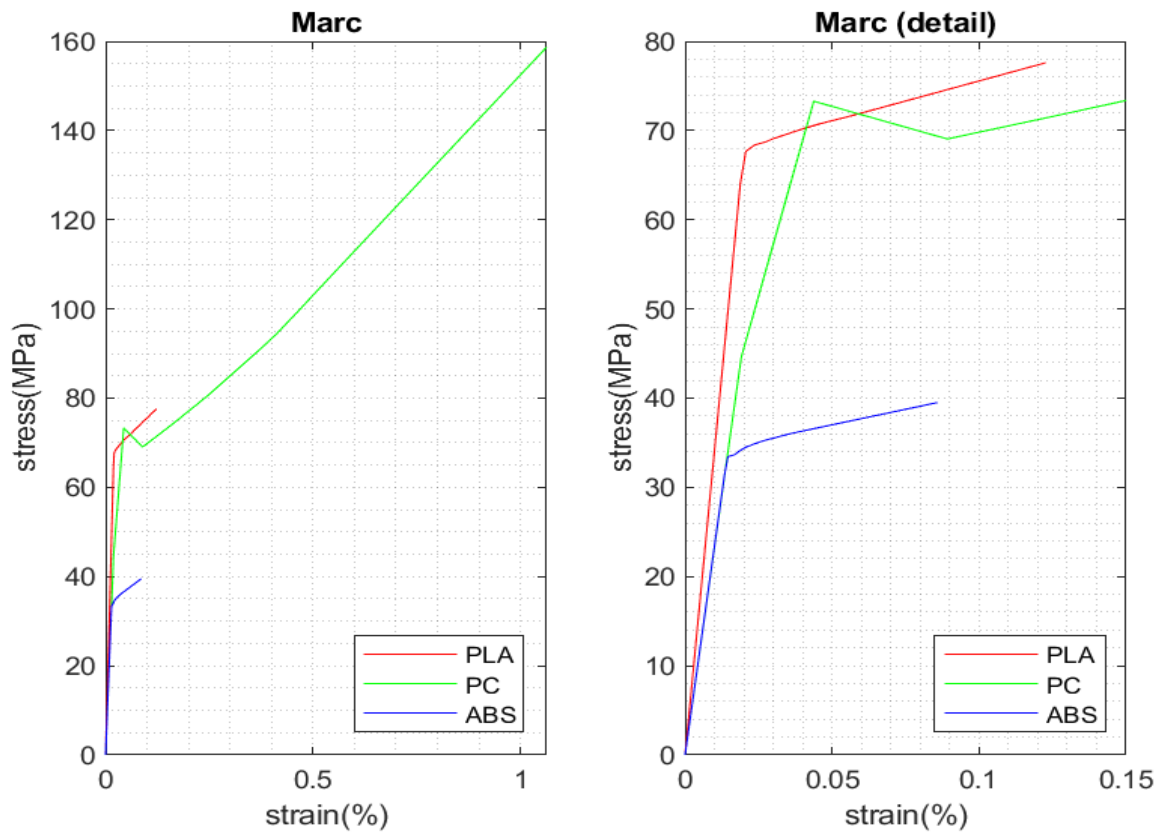


Figure 17. Stress-strain curves obtained using only Marc

Analysing the Fig. 17, it is possible to recognise the elasto-plastic behaviour of the three different materials. PLA and ABS have a similar trend, except for the fact that Yield stress and Young's modulus of ABS are lower. Regarding polycarbonate instead, unlike most thermoplastics, it can undergo large plastic deformations without cracking or breaking in fact, the fixed displacement imposed is higher than the other ones [24].

## 3.2. Digimat model

Compared to the previous curves, in this paragraph the goal is to simulate the mechanical response of specimen in which printing parameters are taken into account and subsequently modified following the model illustrated in Chapter 2. For each test material, representative papers among those listed in Table 1 have been chosen. In order to compare the data, in the present work the same construction parameters adopted by the cited papers have been chosen. In the next lines, results have been divided according to the material used and the different cases have been renamed with the main paper author's name. Regarding the failure of the specimens, the models were not adjusted to consider this aspect while in the experimental case, obviously, the material reaches the failure when the stress is equal to the UTS. Hence, the section of the graph of greatest interest is the linear one. In the following, resulting curves from the

numerical simulations are called ‘*Author’s name\_x*’ and the ones present in the papers ‘*Exp.Author’s name\_x*’ so as to compare easily the two curves. An important observation is that the properties of the materials used in the papers are often not provided and therefore in the model a characteristic value has been introduced. For this reason, it is possible that the curves (experimental and numerical) have different stiffness and strength but this a not relevant problem since what is interesting to observe is the match between trends.

### 3.2.1 Polylactic acid

- **Case study: Ferreira**

The first case analysed considers two different raster angles keeping constant all other parameters as illustrated in Table 4.

	<i>Build orientation</i>	<i>Raster angle</i>	<i>Layer thickness [mm]</i>	<i>Infill pattern [%]</i>
<i>Ferreira_1</i>	Horizontal	0°	0.3	100
<i>Ferreira_2</i>	Horizontal	90°	0.3	100

Table 4. Ferreira et al.’s build parameters [20]

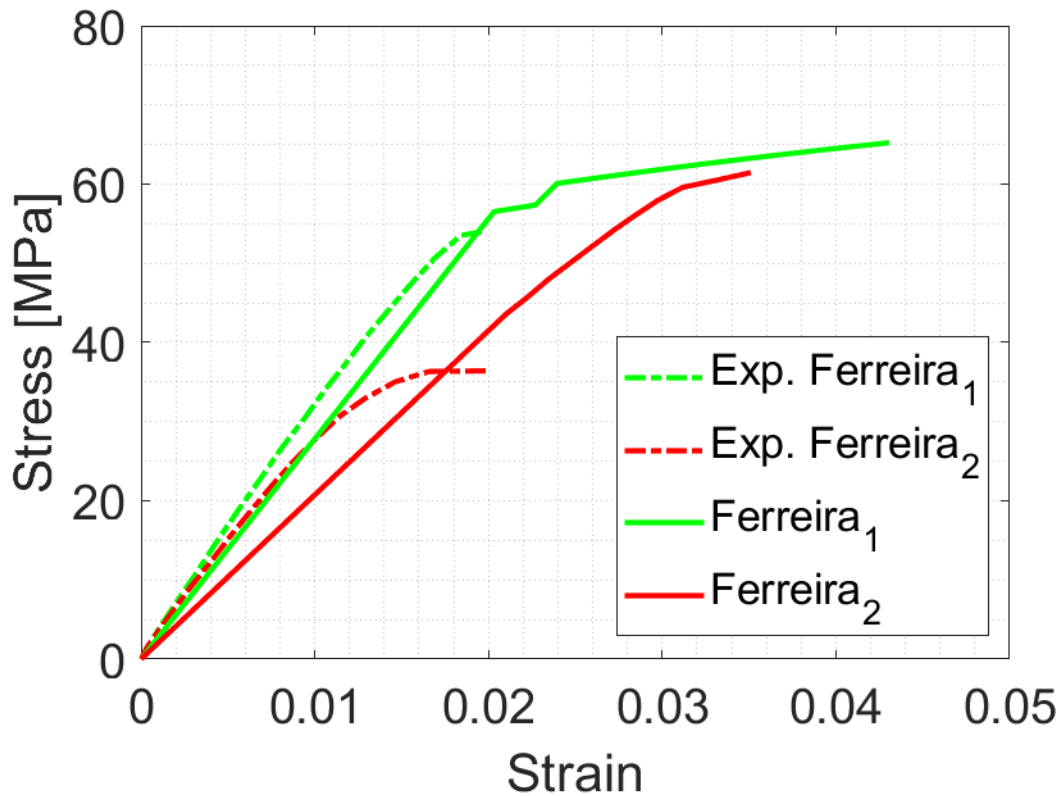


Figure 18. Experimental VS Simulated stress-strain curves of Ferreira case study [20]

As shown in Fig. 18, and according to the experimental curves, in the case of raster angle of  $90^\circ$  the Young's modulus decreases respect to the  $0^\circ$  raster angle. This is may be due to  $0^\circ$  raster angle, all the layers have been deposited parallel to the loading direction of tensile strength. Thus, there is higher stiffness in this case, whereas using  $90^\circ$  the layers are perpendicular to the loading direction and the individual layers are capable to bear less load during tensile test [25].

- **Case study: Chacon**

The aim of this paragraph is to study the influence of the building orientations, the layer thickness and different speed rates on the tensile behaviour. Table 5 reports the description of the different cases studied.

	<i>Build orientation</i>	<i>Raster angle</i>	<i>Layer thickness [mm]</i>	<i>Infill pattern [%]</i>	<i>Speed rate [mm/s]</i>
<i>Chacon_1</i>	Vertical	0°	0.06	100	20
<i>Chacon_2</i>	On-Side	0°	0.06	100	20
<i>Chacon_3</i>	Horizontal	0°	0.06	100	20
<i>Chacon_4</i>	Vertical	0°	0.24	100	20
<i>Chacon_5</i>	On-Side	0°	0.24	100	20
<i>Chacon_6</i>	Horizontal	0°	0.24	100	20
<i>Chacon_7</i>	Vertical	0°	0.06	100	80
<i>Chacon_8</i>	On-Side	0°	0.06	100	80
<i>Chacon_9</i>	Horizontal	0°	0.06	100	80
<i>Chacon_10</i>	Vertical	0°	0.24	100	80

---

<i>Chacon_11</i>	On-Side	0°	0.24	100	80
<i>Chacon_12</i>	Horizontal	0°	0.24	100	80

---

*Table 5. Chacon et al.'s build parameters [7]*

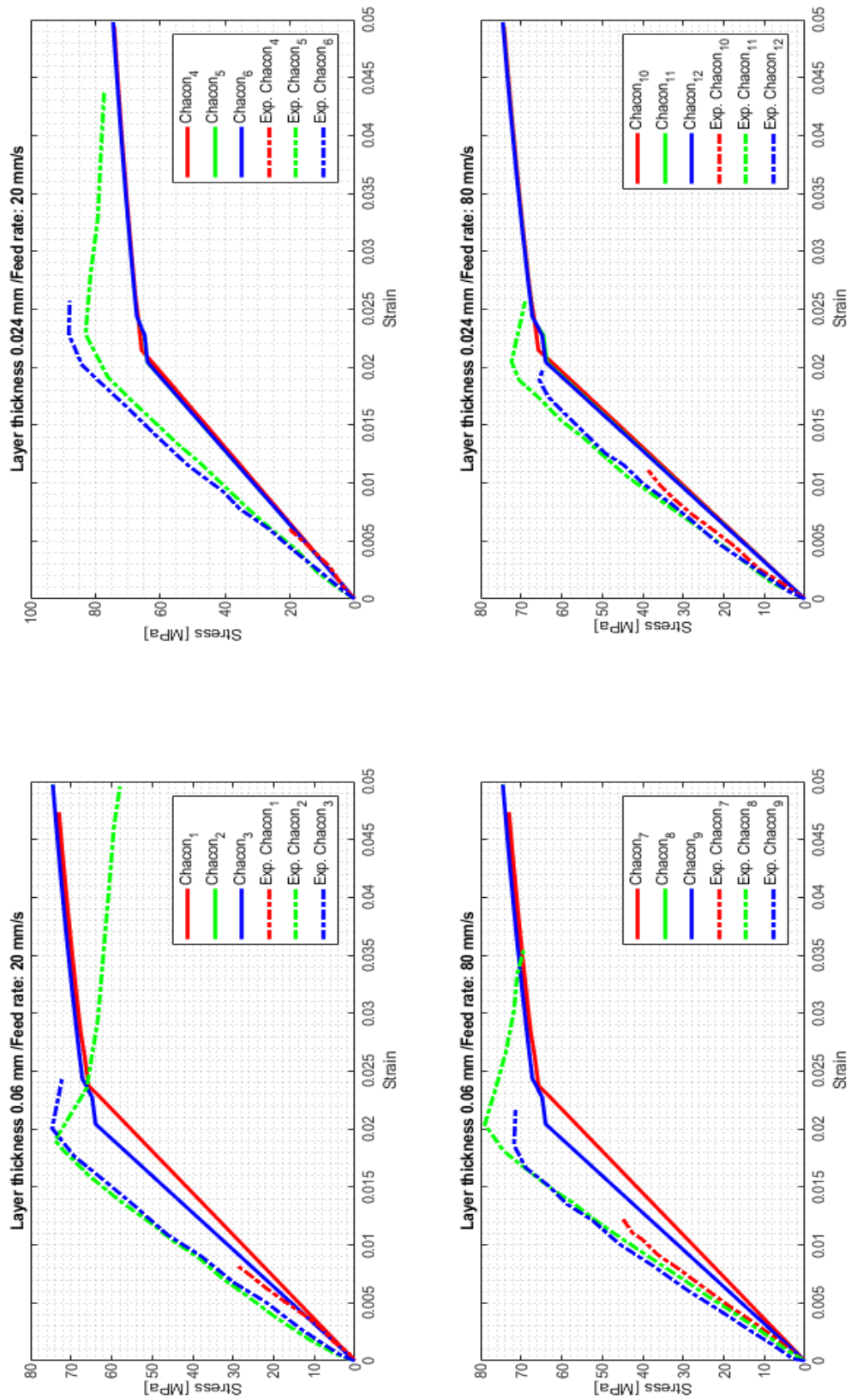


Figure 19. Experimental VS Simulated stress-strain curves of Chacon case study [7]

As expected, PLA printed test specimens shows a remarkable anisotropy: horizontal and on-side specimen have the highest values for tensile strengths and stiffness. This can be explained because in vertical specimen the load is perpendicular to their fibers resulting in inter-layer fusion bond failure while flat and horizontal specimen show a trans-layer failure [7]. Both in the experimental case and in the simulated one, the effect of layer thickness is different depending on the build orientation. In the case of vertical samples, the strength increases as layer thickness increases. In the case of horizontal and on-side samples, the variations of tensile behaviour with changes in layer thickness are marginally significance. The effect of speed rate whilst, has not a great influence on the mechanical properties. As it is possible to see in Fig. 19, the trend of the numerical data match with the experimental one.

- **Case study: Rodriguez**

The last case study for PLA investigates the effect of build orientation, raster orientation, layer thickness and infill pattern. The first set is the reference case with respect to this the parameters are changed to observe the variations.

---

	<i>Build orientation</i>	<i>Raster angle</i>	<i>Layer thickness [mm]</i>	<i>Infill pattern [%]</i>
<i>Rodriguez_1</i>	Horizontal	±45°	0.1	20

---

<i>Rodriguez_2</i>	Horizontal	$\pm 45^\circ$	0.2	20
<i>Rodriguez_3</i>	Horizontal	$\pm 45^\circ$	0.1	50
<i>Rodriguez_4</i>	Vertical	$\pm 45^\circ$	0.1	20
<i>Rodriguez_5</i>	On-Side	$\pm 45^\circ$	0.1	20

Table 6. Rodriguez et al.'s build parameters [19]

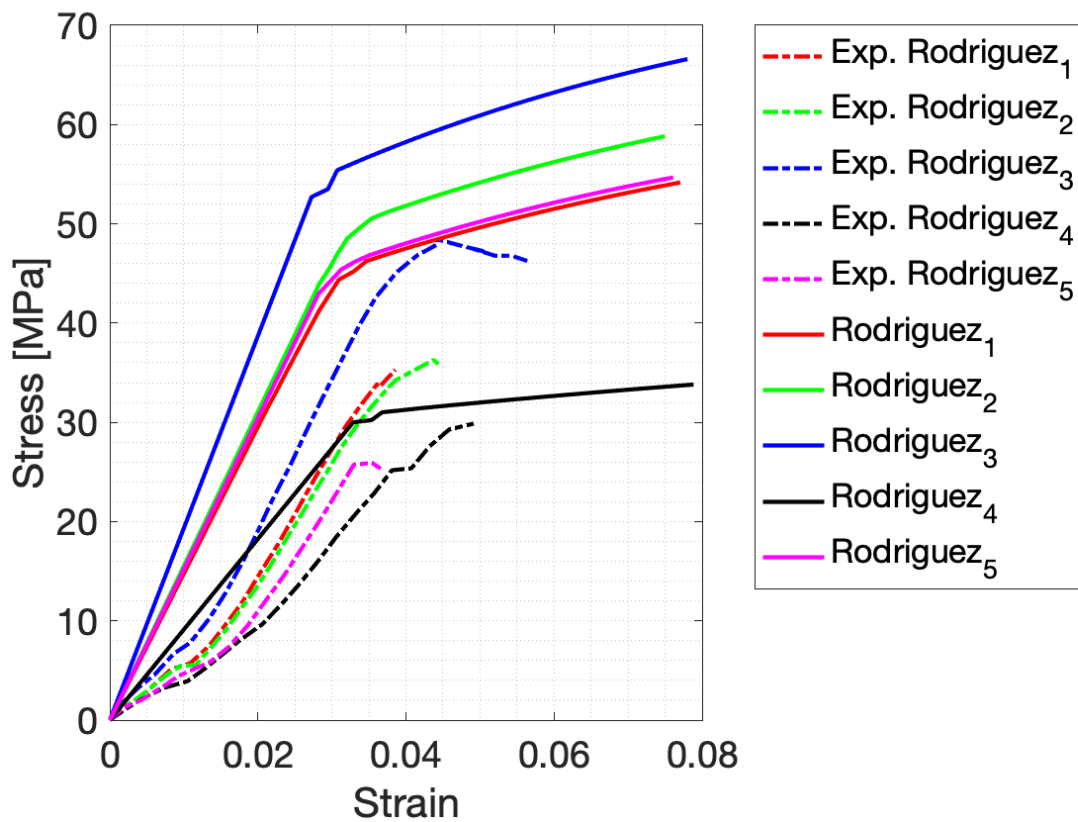


Figure 20. Experimental VS Simulated stress-strain curves of Rodriguez case study [19]

On the graph shown in Fig. 20, the simulated curves do not fit the slope because the properties of the material used for the tests are unknown and average values were introduced. Curves have to be analysed considering the colour match. For example, it is possible to see how the Rodriguez<sub>3</sub> curve is the highest both in the numerical and the experimental case. This agrees with what is expected since it is the case with the highest infill density. The same comment can be done for Rodriguez<sub>4</sub> where the samples are manufactured in vertical direction. As explained for Chacon case study, the load is perpendicular to the fibers and, the failure is an inter-layer failure. Unlike Chacon case, however, in this study the decrease of stiffness and strength of vertical samples with respect to the horizontal and on-side case, is much more marked. This aspect can be explained since the infill pattern in this case is 20% and not 100% as Chacon, and so the phenomena of loss of resistance is greater because the porosity is higher. For the remaining cases, a first conclusion is that the model is not able to point out differences between the on-side and the horizontal samples unlike experimental tests. This may be due to the definition of the loading and printing orientations that are equal in both cases.

### **3.2.2. Acrylonitrile butadiene styrene**

- **Case study: Riddick**

The following analysis is relative to ABS manufactured specimen in which build orientation and raster angle are changed as showed in the next Table.

	<i>Build orientation</i>	<i>Raster angle</i>	<i>Layer thickness [mm]</i>	<i>Infill pattern [%]</i>
<i>Riddick_1</i>	On-Side	0°	0.127	100
<i>Riddick_2</i>	Horizontal	0°	0.127	100
<i>Riddick_3</i>	Vertical	0°	0.127	100
<i>Riddick_4</i>	On-Side	90°	0.127	100
<i>Riddick_5</i>	Horizontal	90°	0.127	100
<i>Riddick_6</i>	Vertical	90°	0.127	100
<i>Riddick_7</i>	On-Side	±45°	0.127	100
<i>Riddick_8</i>	Horizontal	±45°	0.127	100
<i>Riddick_9</i>	Vertical	±45°	0.127	100

*Table 7. Riddick et al.'s build parameters [11]*

As in the previous examples, experimental and numerical curves are compared to each other in Fig. 21 to study the validity of the method.

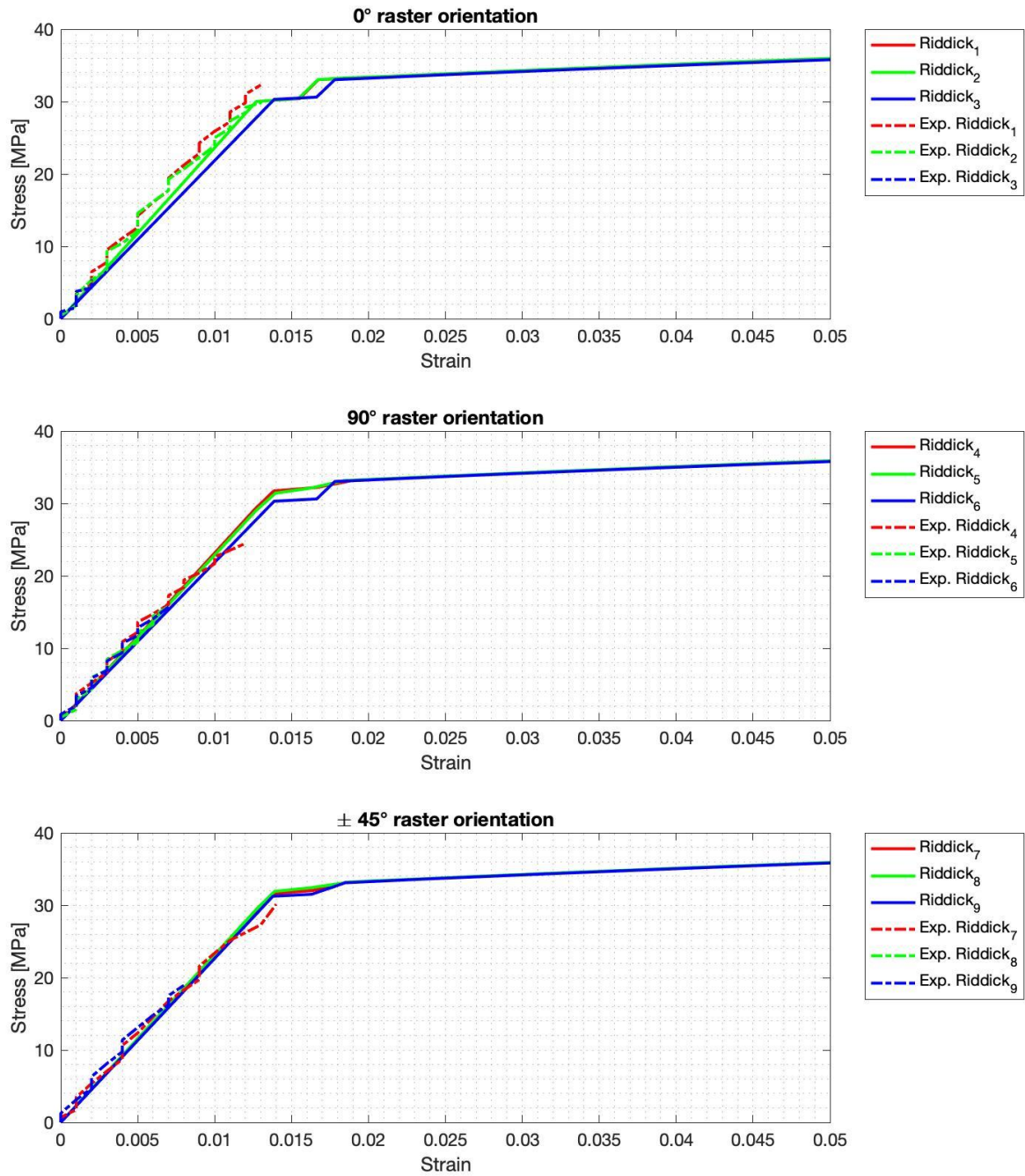


Figure 21. Experimental VS Simulated stress-strain curves of Riddick case study [11]

Both in the experimental and in the numerical case, the curves tend to overlap. In this case the model shows a very good result probably due to a better knowledge of the material properties of the experimental test reported in the paper [11]. *Riddick et al.* [11], observe that the stress-strain response of the  $\pm 45^\circ$  specimens were characterized by evident softening due to the shear response, resulting in the greatest elongation-at-break value of all the specimens tested. This phenomenon it is not evident in the results from the simulation because, as previously mentioned, the model does not consider the failure and all the curves have the same elongation at break that is the one fixed as boundary condition in Marc. With respect to the Chacon case, the three building orientations (horizontal, on-side and vertical) do not show significative differences and this is due to the higher layer thickness.

- **Case study: Cantrell**

To validate the proposed model also for ABS made specimens, another paper has been studied. The parameters are the same of the last three cases of the previous one.

	<i>Build orientation</i>	<i>Raster angle</i>	<i>Layer thickness [mm]</i>	<i>Infill pattern [%]</i>
<i>Cantrell_1</i>	Horizontal	$\pm 45^\circ$	0.1	100
<i>Cantrell_2</i>	On-side	$\pm 45^\circ$	0.1	100

<i>Cantrell_3</i>	Vertical	$\pm 45^\circ$	0.1	100
-------------------	----------	----------------	-----	-----

Table 8. Cantrell et al.'s build parameters [17]

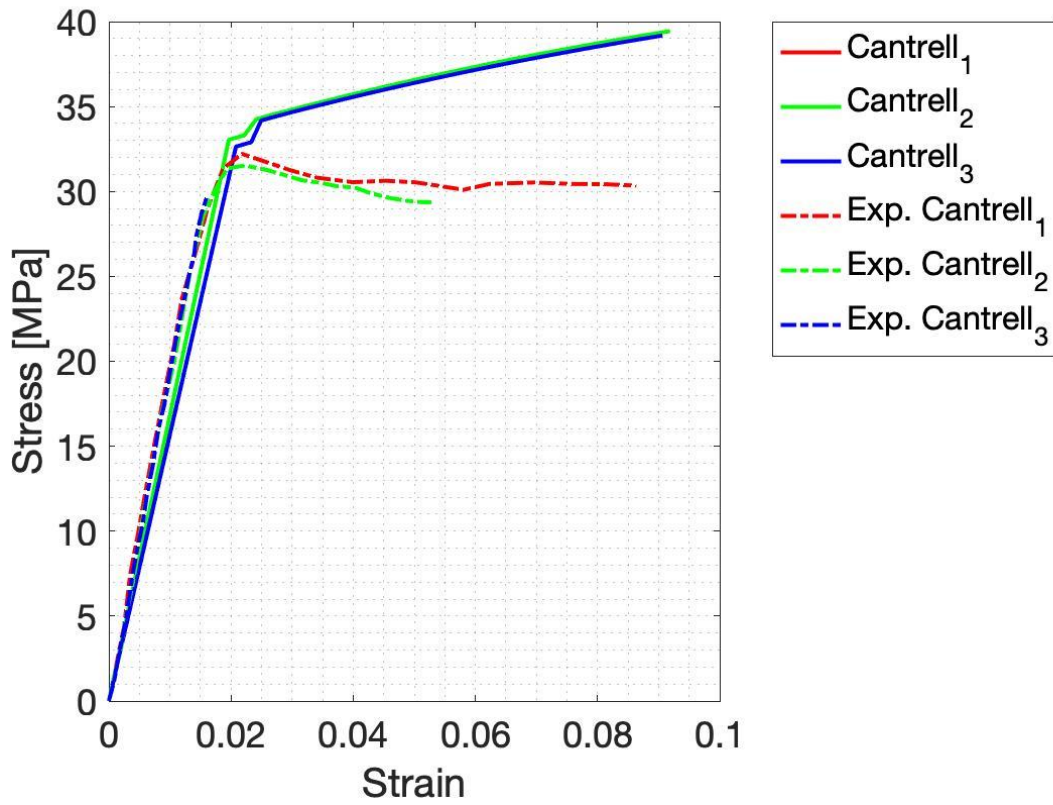


Figure 22. Experimental VS Simulated stress-strain curves of Cantrell case study [17]

As in the previous case, curves fit very well the slope; small differences can be observed in the plasticity phase where the material behaviour is difficult to simulate. From here, it is highlighted the need to know the exact characteristic of the material used to simulate the real one. Optionally, it is also possible testing the filament or an injection-moulded specimen because the materials datasheet often is misleading, as demonstrated by *Rodriguez et al.* [19]. Beyond these

---

considerations, also in this study it is possible to observe an interesting match in the linear part.

### 3.2.3. Polycarbonate

- **Case study: Domingo**

The last papers study the Polycarbonate. Considering the different behaviour of this thermoplastic, the showed case investigates the effect of the modification only in build direction, Table 9.

	<i>Build orientation</i>	<i>Raster angle</i>	<i>Layer thickness [mm]</i>	<i>Infill pattern [%]</i>
<i>Domingo_1</i>	Horizontal	$\pm 45^\circ$	0.2	100
<i>Domingo_2</i>	On-Side	$\pm 45^\circ$	0.2	100
<i>Domingo_3</i>	Vertical	$\pm 45^\circ$	0.2	100

Table 9. Domingo et al.'s build parameters [15]

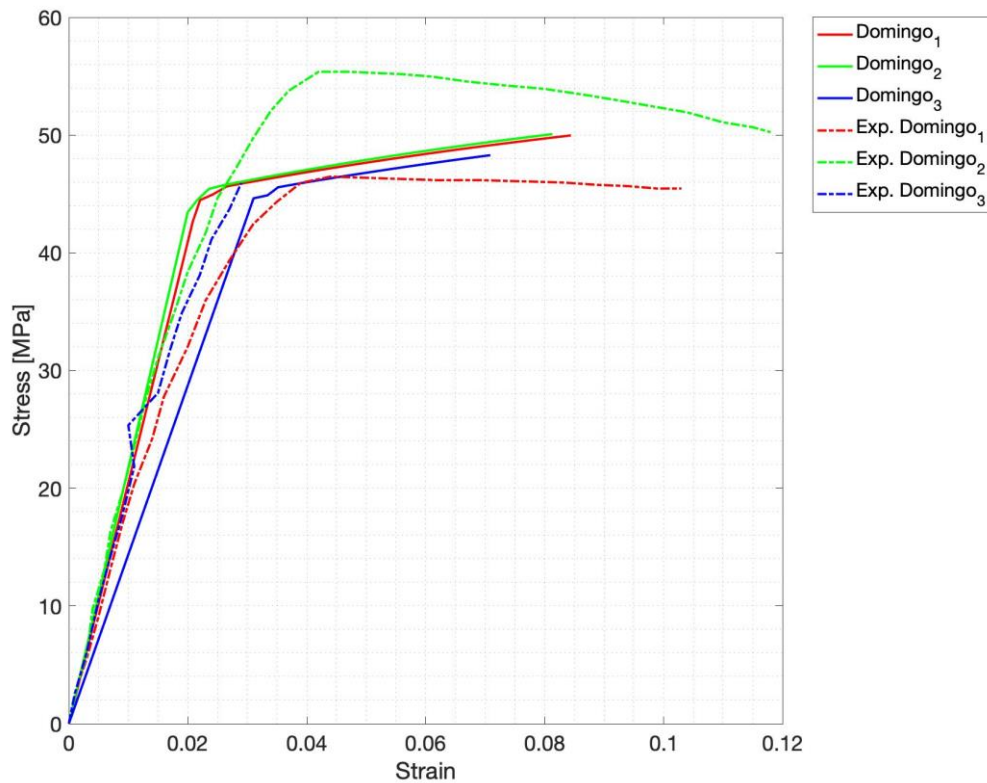


Figure 23. Experimental VS Simulated stress-strain curves of Domingo case study [15]

Analysing the curves in Fig. 23, simulated ones present a trend in agree with the theory. In fact, the horizontal case has the highest Young's modulus and Yield stress, followed by the on-side samples and the vertical one. In the paper used for the validation, this trend is not respected in fact the horizontal case is the worst. This is in contrast with the literature until now, the testing procedure and the material used should be better investigate to be sure of the validation.

- **Case study: Salazar**

The second paper found for PC made specimens considers three different air gap and numbers of contours, as shown in Table 10. Other FDM process were kept constants, also because they have been already been extensively investigated in the previous works.

	<i>Build orientation</i>	<i>Raster angle</i>	<i>Layer thickness [mm]</i>	<i>Infill pattern [%]</i>	<i>Numbers of contours</i>
<i>Salazar_1</i>	Horizontal	0°	0.254	100	1
<i>Salazar_2</i>	Horizontal	0°	0.254	100	5
<i>Salazar_3</i>	Horizontal	0°	0.254	100	10
<i>Salazar_4</i>	Horizontal	0°	0.254	60	1
<i>Salazar_5</i>	Horizontal	0°	0.254	60	5
<i>Salazar_6</i>	Horizontal	0°	0.254	60	10
<i>Salazar_7</i>	Horizontal	0°	0.254	30	1
<i>Salazar_8</i>	Horizontal	0°	0.254	30	5
<i>Salazar_9</i>	Horizontal	0°	0.254	30	10

Table 10. Salazar et al.'s build parameters [14]

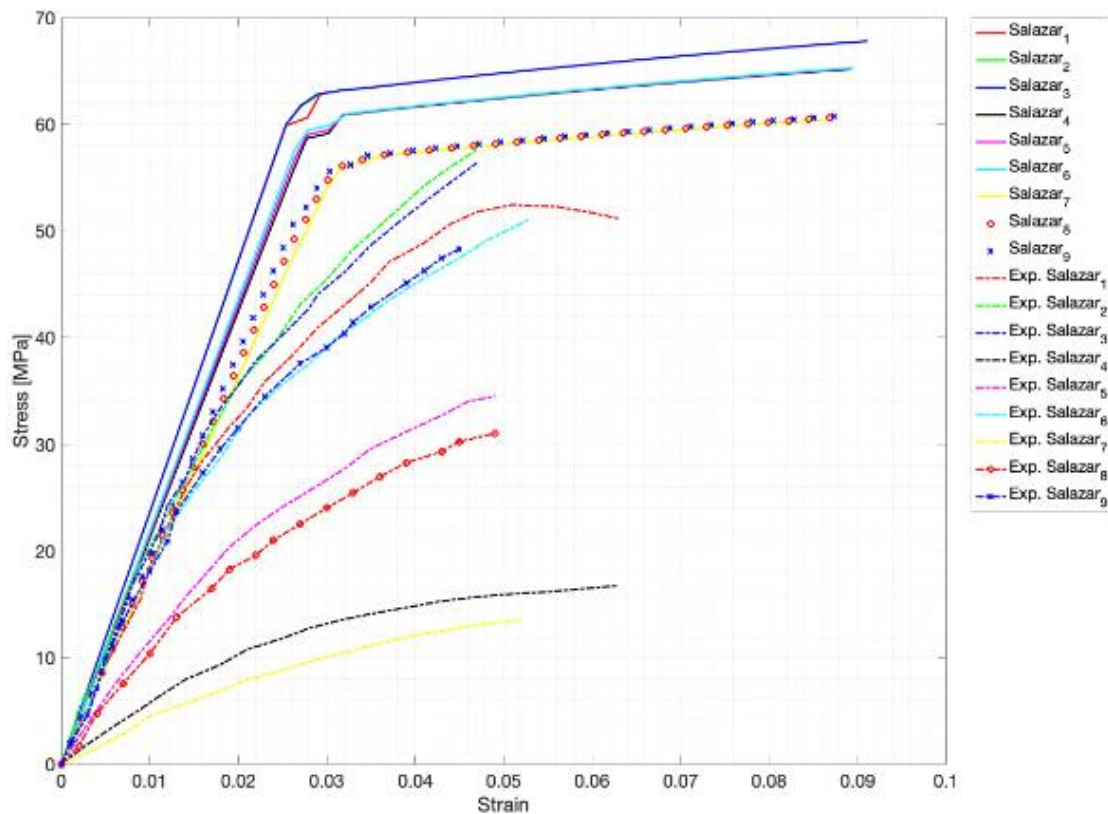


Figure 24. Experimental VS Simulated stress-strain curves of Salazar case study [14]

In Fig. 24, the model's answer regarding the changes in the air gap is in accordance with what is expected in fact, as the air gap increases, the stiffness and the Yield stress decrease. Nevertheless, in the case of the number of contours variation, the model is not able to show some differences, and this is evident from the total overlapping of the curves in the three cases. A plausible explanation can be found in the definition of the toolpath in Cura. During the mapping, the donor mesh is the G-Code file and this is needed to change the receiving mesh with the manufacturing data. This is particularly significant if the infill pattern is changed in terms of percentage but with the increasing of the contours, the printed information is not efficiently transferred.

### 3.3. Experimental validation

Once the model has been validated with the results from literature, a laboratory test was performed. Samples were manufactured according to the ASTM D638 standard method for tensile properties. The printer used is the Ultimaker 3 extended and, the Cura software has been used to export the three-dimensional models of the samples to G-code. The STL file has been generated on Solidworks following the dimensions of Type I specimen ( $l=165$  mm,  $w= 13$  mm,  $t= 4$  mm). The material used is PLA and its characteristics are provided by the manufacture [28]. For the printing parameters, Rodriguez<sub>1</sub> and Rodriguez<sub>4</sub> have been chosen; both the samples were manufactured with an infill of 20% and a raster angle of  $\pm 45^\circ$  but, the first one is horizontal and the second one vertical. These two examples were chosen with the purpose of validate the model with a specimen with a low infill option. One of the biggest challenges is to predict the controlled porosity material behaviour starting from bulk materials properties. Table 11 shows the printing criteria of the two specimens and in Fig. 25 it is possible to see the building platform with the samples anchored to it. For each case, five samples were printed as specified in the standard.

	<i>Build orientation</i>	<i>Raster angle</i>	<i>Layer thickness [mm]</i>	<i>Infill pattern [%]</i>
<i>Rodriguez_1</i>	Horizontal	$\pm 45^\circ$	0.2	20
<i>Rodriguez_4</i>	Vertical	$\pm 45^\circ$	0.2	20

Table 11. Printing parameters of the laboratory test [19]

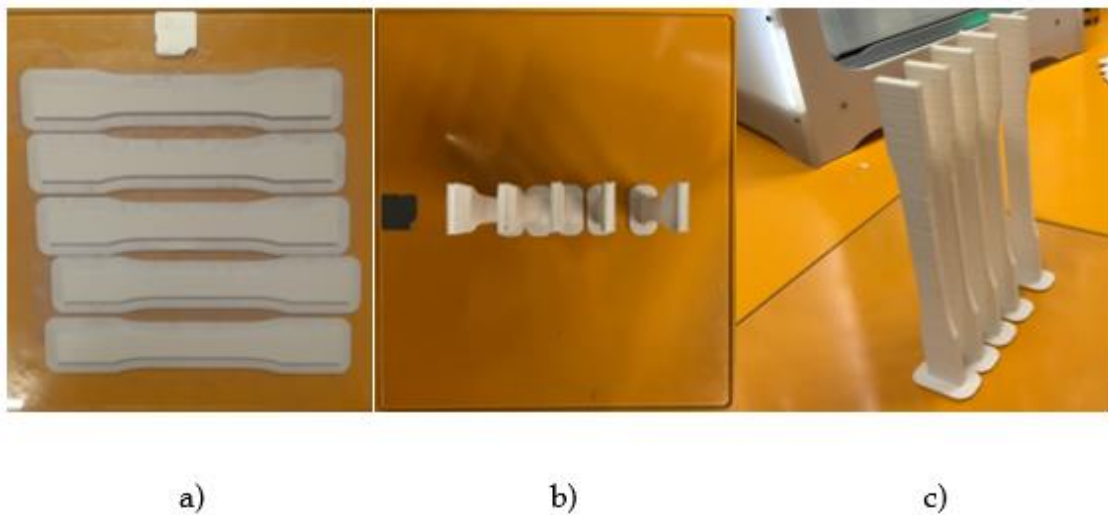


Figure 25. Specimens anchored to the platform: a) horizontal specimens b) vertical specimens top view c) vertical specimens 3D view

The uniaxial tensile tests were performed using an ElectroForce 3500 electro-mechanical testing machine with a fixed rate of 1 mm/min (Fig. 26).



Figure 26. ElectroForce 3500 series Universal testing machine

First samples tested were the horizontal ones. Data acquired during the tests are the load and the crosshead displacement. To obtain the stress, the load has been divided to the cross-sectional area of the specimen equal to 52 mm. Fig. 27 shows the PLA specimens tested after the test.

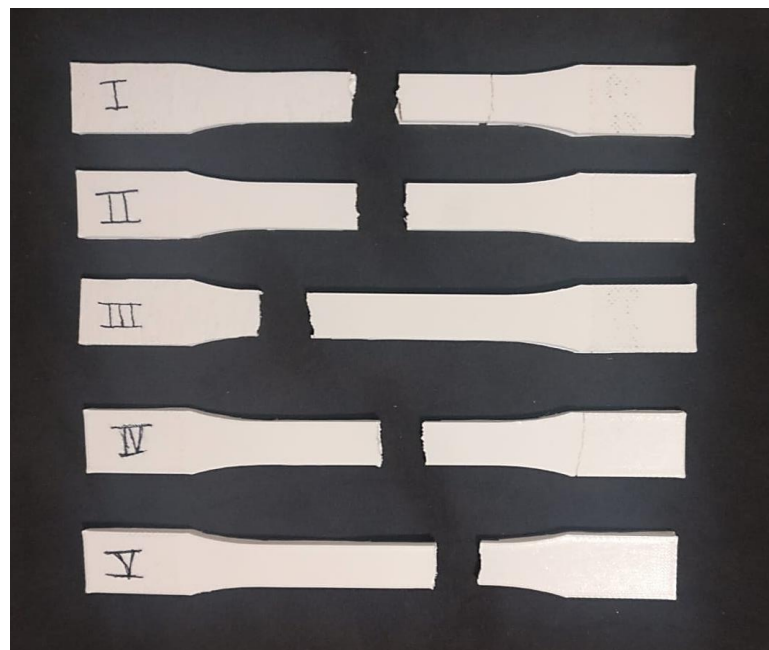
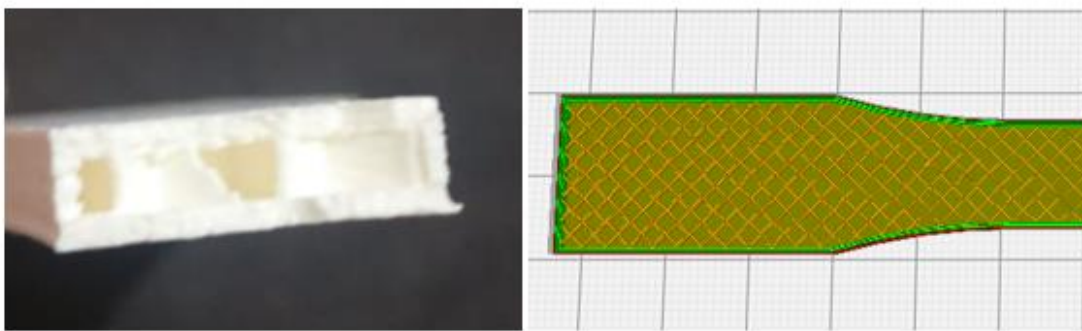


Figure 27. PLA test specimens tested

Due to the layers orientation in the direction of the stress and the raster angle of the infill of  $\pm 45^\circ$ , a rupture with an irregular breakage lines can be observed [19]. Specimens I and IV exhibit a second breakage because of the bounce of the inferior crosshead after the fracture. A detail of the fracture surface (a) and the infill obtained in Cura (b) is presented in Fig. 28.



*Figure 28. a) Fracture surface b) infill option*

The aim of the laboratory test is to compare the Digimat simulated curve with the ones achieved from the uniaxial tensile test. As anticipated before, the model is not able to predict the failure and therefore the unique interesting section to compare is the linear one. Fig. 29 shows the results obtained. A first consideration is the repeatability of the five specimens that confirms the accuracy of the tests. Moreover, the model shows a good match with the experimental curves since the error between the two curves is 3.2%.

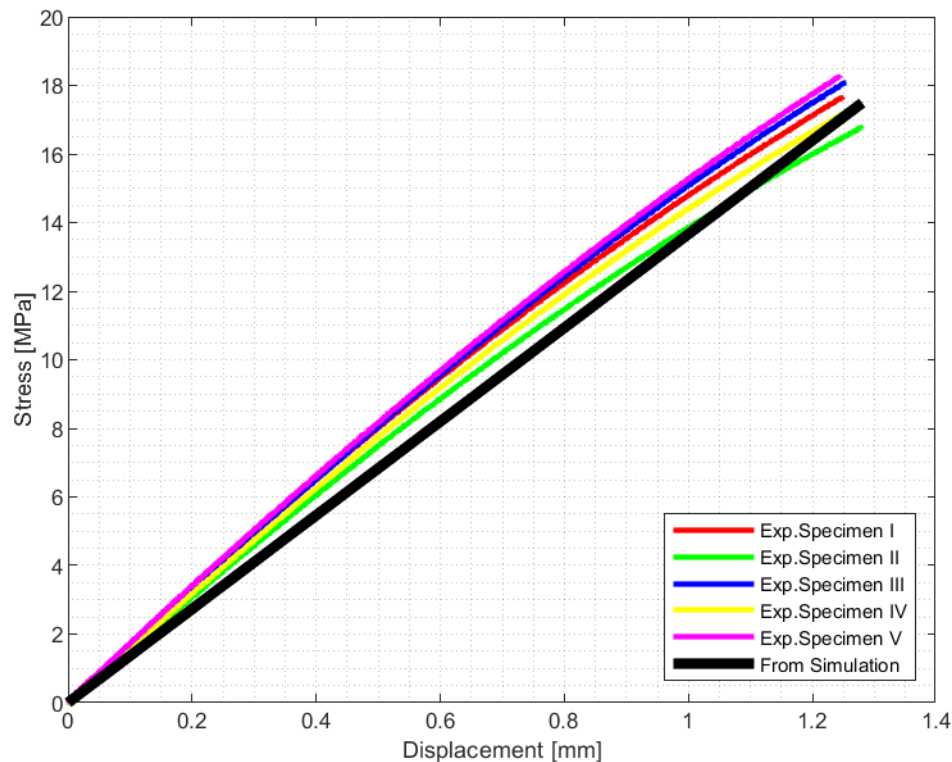


Figure 29. Simulated VS Experimental curves of horizontal samples tested in laboratory

The validation can be defined acceptable: the curve obtained from the simulation can provide good results without testing the samples and a consistent variation with the respect to the solid specimen.

The second laboratory test kept constant the equipment and the printing parameters except for the build orientation, in this case vertical. One of the biggest issues of this experiment was the printing of the samples. Fig. 30 shows the major defects of the components: on the top it is highlighted a variation in the filament deposition while in the bottom a lack in the contour closing is clearly visible and this is probably due to a low value of wall thickness. Another

problem was observed after the specimen breakage, because to some difficulties of the printing process and to a bad running of the printer, the infill raster angle of  $\pm 45^\circ$  wasn't respected. In Fig. 31 differences between the Cura file and the real specimen are showed.



Figure 30. Defects of vertical printed component: on the top, different in the filament deposition; on the bottom, contour problems

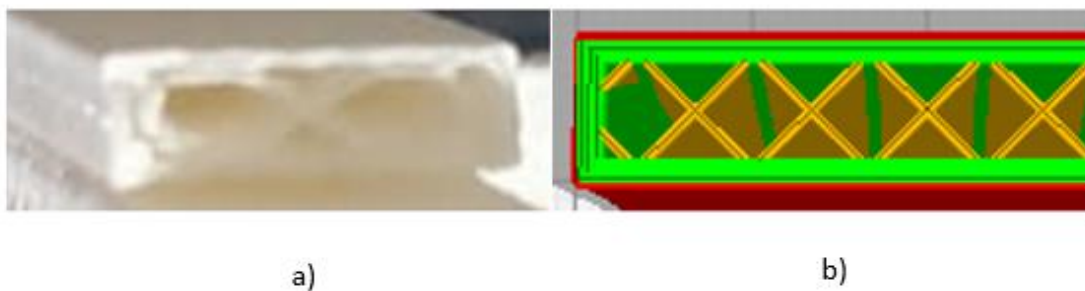


Figure 31. Different infill: a) printed specimen b) from Cura software

How could it be expected because of all these defects, results obtained from the tensile test are not reliable and only one specimen has been tested. Fig. 32 reports the curve where the maximum strength is 2.5 kN, value obviously non acceptable.

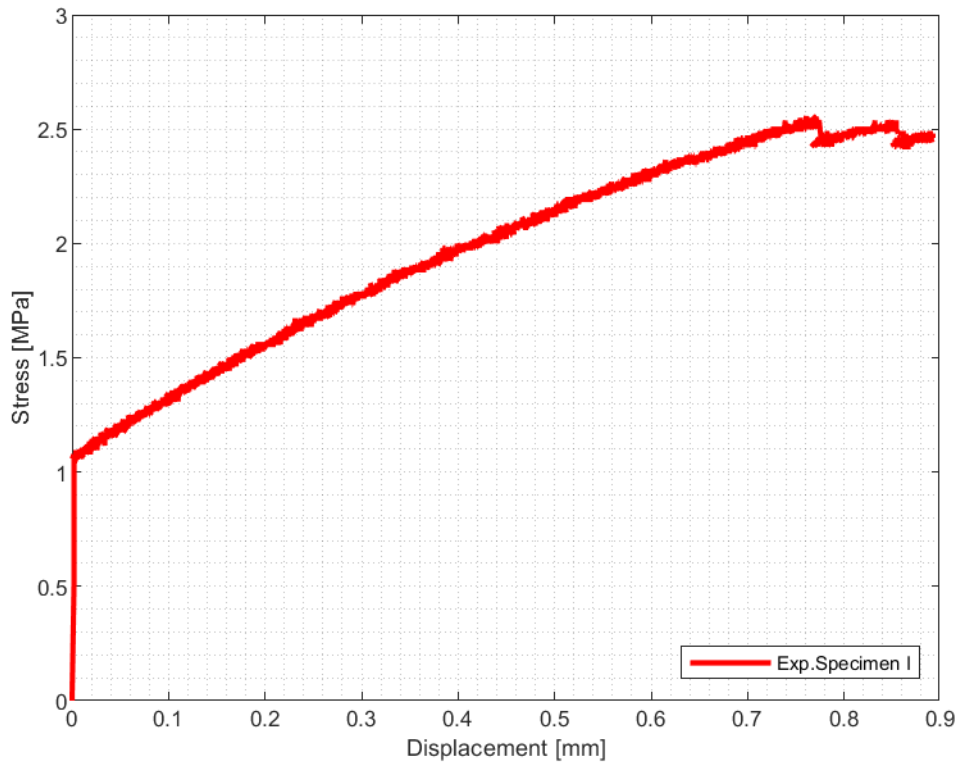


Figure 32. Experimental curve of vertical sample tested in laboratory

## Chapter 4: Conclusions

Components made by FDM are influenced by printing parameters. The aim of this work was to predict the mechanical behaviour of FDM made specimens using a coupled analysis of Digimat with a FEA solver. The tensile behaviour of the material is the only analysed in this work.

The proposed model uses DIGIMAT to characterize the structural model of the specimens with the material porosity and the manufacturing data. Stress-strain curves extrapolated from the simulations have been validate with experimental results from the literature and laboratory tests. One of the relevant results is that the model clearly differentiates vertical and horizontal samples. A common outcome present in literature is that the specimen manufactured in vertical direction have lower properties because the load is applied perpendicular to the fibers. This behaviour is always respected in the results of the presented model. Regarding the differences between horizontal and on-side samples in contrast, from the simulated curves it is not possible to appreciate some differences even if the experimental tests often show small variations. This may be because of the description of the printing and loading directions in the material definition are equal in both cases.

Regarding the variations of infill density and layer thickness, the simulated curves are in agree with the trend of the experimental ones. For example, increasing the infill density, the Young's modulus and the Yield stress rise as expected since there is more area on which force can be applied. Because of this study it can be concluded that the implemented model shows a good match with the experimental results regarding the variation between the vertical and the horizontal samples and the changes in the infill density and layer thickness. This is particularly useful to simulate and understand the final behaviour of FDM printed specimens without testing them. One interesting conclusion is the importance of knowing the exact material properties (i.e. Young's modulus, Yield stress) to better simulate the behaviour.

In future works, it could be interesting studying also the failure system at different printing parameters and considering the flexural and impact behaviour.

## Appendix

The latest DIGIMAT versions offer a product called DIGIMAT-AM that is dedicated to the additive manufacturing process simulation of polymers and composite materials. This solver is able to predict the warpage, residual stresses, temperature history and microstructure changes that undergo a printed part [1]. During the mapping process, it is possible to map not only the manufacturing data but also the file contained the information about the residual stresses. The same workflow illustrated in Chapter 2 is followed. Here an example of this approach is reported.

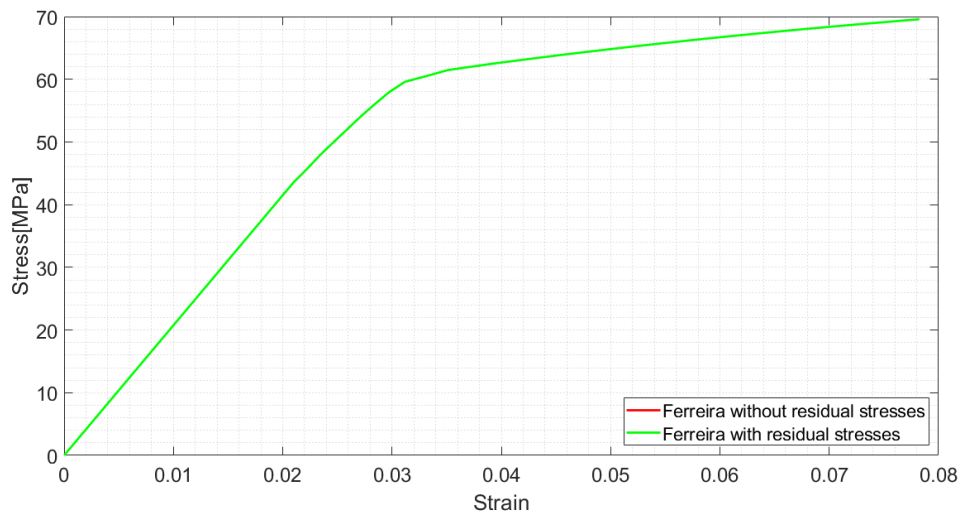


Figure 33. Effect of the residual stresses

As it is possible to see from the total overlapping of the two curves in Fig. 33, residual stresses do not influence the behaviour. For this reason, they are not considered in the proposed model.

## References

- [1] Digimat 2019 manual
- [2] A. Gebhardt, "Rapid Prototyping-Rapid Tooling-Rapid Manufacturing", Carl Hanser, München, 2007.
- [3] "Additive manufacturing – General Principles – Overview of process categories and feedstock". ISO/ASTM International Standard. 17296-2:2015(E). 2015.
- [4] I. Gibson, D. Rosen, B. Stucker, Additive Manufacturing Technologies: 3D Printing, Rapid Prototyping and Direct Digital Manufacturing. 2nd ed., Springer. 2014.
- [5] Available on-line: [www.custompartner.com](http://www.custompartner.com)
- [6] Ryan Neal Kay, "Effect of Raster Orientation on the Structural Properties of Components Fabricated by Fused Deposition Modeling", Thesis, 2014.
- [7] J.M. Chacòn, et al., "Additive manufacturing of PLA structures using fused deposition modelling: Effect of process parameters on mechanical properties and their optimal selection", Mater. Des 124 (2017)
- [8] D. Croccolo, et al., "Experimental characterization and analytical modelling of the mechanical behaviour of fused deposition processed parts made of ABS-M30", Computational Material Science 79 (2013)

- [9] T. W. Kerekes, et al., "Characterization of process-deformation/damage property relationship of fused deposition modelling (FDM) 3D-printed specimens", *Addit. Manuf.* 25 (2019)
- [10] S. Ahn, et al., "Anisotropic material properties of fused deposition modeling ABS, *Rapid Prototyping*", Vol. 8 · Number 4 · 2002 ·
- [11] J. Riddick, et al., "Fractographic analysis of tensile failure of acrylonitrile-butadiene-styrene fabricated by fused deposition modeling", *Addit. Manuf.* 11 (2016)
- [12] S. Ravindrababu, et al., "Evaluation of the influence of build and print orientations of unmanned aerial vehicle parts fabricated using fused deposition modeling process", *Journal of Manufacturing Processes* 34 (2018)
- [13] Available on-line: [www.stratasys.com](http://www.stratasys.com)
- [14] A. Salarz-Martin et al., "A study of creep in polycarbonate fused deposition modelling parts", *Materials and design* (2018).
- [15] M. Domingo-Espin et al., "Mechanical property characterization and simulation of fused deposition modeling Polycarbonate parts", *Materials & Design* (2015) 10.1016
- [16] Standard Test Method for Tensile Properties of Plastics
- [17] Cantrell and Rohde, "Experimental characterization of the mechanical properties of 3D-printed ABS and polycarbonate parts" *Rapid Prototyping Journal* (2017)

- [18] M. Samykano et al., "Mechanical property of FDM printed ABS: influence of printing parameters", *The International Journal of Advanced Manufacturing Technology* (2019)
- [19] A. Rodriguez-Panes et al., "The influence of Manufacturing parameters on the mechanical behaviour of PLA and ABS pieces manufactured by FDM: a comparative analysis", *materials* (2018)
- [20] R. Ferreira et al, "Experimental characterization and micrography of 3D printed PLA and PLA reinforced with short carbon fibers", *Composites Part B* (2017),
- [21] Available online: [www.markummittchell.github.io/engauge-digitizer/](http://www.markummittchell.github.io/engauge-digitizer/)
- [22] Available online: [www.mscsoftware.com/product/digmat](http://www.mscsoftware.com/product/digmat)
- [23] Eduardo Pedro, "Structural analysis of Injection molded components using Digimat as interface software" (2017)
- [24] Behzad et al., "Simulation of mechanical behavior and optimization of simulated injection molding process for PLA based antibacterial composite and nanocomposite bone screws using central composite design", *ScienceDirect* (2017)
- [25] Available online: [www.matweb.com](http://www.matweb.com)
- [26] Available on-line: Wikipedia
- [27] Shilpesh R. and Harshit K., "Analysis of tensile strength of a fused filament fabricated PLA part using an open-source 3D printer", *The International Journal of Advanced Manufacturing Technology* (2018)

[28] Technical datasheet PLA, Ultimaker